Journal of Electromyography and Kinesiology 76 (2024) 102873

Contents lists available at ScienceDirect

Journal of Electromyography and Kinesiology

journal homepage: www.elsevier.com/locate/jelekin

NeuroMechanics: Electrophysiological and computational methods to accurately estimate the neural drive to muscles in humans *in vivo*

Arnault H. Caillet [a], Andrew T.M. Phillips [b], Luca Modenese [c,1,*], Dario Farina [a,1,*]

[a] Department of Bioengineering, Imperial College London, UK
[b] Department of Civil and Environmental Engineering, Imperial College London, UK
[c] Graduate School of Biomedical Engineering, University of New South Wales, Sydney, Australia

ARTICLE INFO

Keywords:
Neural drive
Motor unit
Motoneuron
muscle control
motor unit population
neuromuscular
high-density EMG
electromyography
electrophysiological methods
computational methods

ABSTRACT

The ultimate neural signal for muscle control is the neural drive sent from the spinal cord to muscles. This neural signal comprises the ensemble of action potentials discharged by the active spinal motoneurons, which is transmitted to the innervated muscle fibres to generate forces. Accurately estimating the neural drive to muscles in humans *in vivo* is challenging since it requires the identification of the activity of a sample of motor units (MUs) that is representative of the active MU population. Current electrophysiological recordings usually fail in this task by identifying small MU samples with over-representation of higher-threshold with respect to lower-threshold MUs. Here, we describe recent advances in electrophysiological methods that allow the identification of more representative samples of greater numbers of MUs than previously possible. This is obtained with large and very dense arrays of electromyographic electrodes. Moreover, recently developed computational methods of data augmentation further extend experimental MU samples to infer the activity of the full MU pool. In conclusion, the combination of new electrode technologies and computational modelling allows for an accurate estimate of the neural drive to muscles and opens new perspectives in the study of the neural control of movement and in neural interfacing.

1. Introduction

Skeletal muscles are multiscale structures composed of individual units called motor units (MUs). A MU comprises a motoneuron (MN) and the muscle fibres it innervates (Heckman & Enoka, 2012). The neural drive to muscle refers to the ensemble of action potentials discharged by the active MN population and transmitted to the muscle fibres (Farina et al., 2014a). At the muscle-scale, the neural drive is seen as the compound neural control signal from the MN pool, which is received by the macroscopic muscle actuator. Therefore, at the muscle-scale, the neural drive represents the sum of the MNs' discharge activities, which is commonly mathematically described as the temporal cumulative series of MNs' discharges. The neural drive at muscle-scale is commonly filtered at frequencies up to 4-to-10 Hz (Farina & Negro, 2015; Enoka & Farina, 2021) because the dynamic response of muscles has small bandwidth.

The intensity of the neural drive is determined by the number of active MNs (recruitment) and their firing rates (rate coding). The recruitment and rate coding dynamics of the MN pool are determined by the amplitude of the net excitatory synaptic drive the MNs receive and on the intrinsic excitability of the MNs, which is influenced by neuromodulatory inputs (Lee et al., 2003; Heckman & Enoka, 2012; Binder et al., 2020; Avrillon et al., 2023a). In response to a rising net excitatory synaptic drive, the MUs are recruited sequentially in order of size (Henneman's size principle; Henneman, 1957; Henneman, 1981), starting with the smallest MUs (small MNs, low rheobase and force thresholds for recruitment, low generated forces). Human MU pools include many low-threshold MUs and few high-threshold MUs following an exponential continuous distribution (Feiereisen et al., 1997; Van Cutsem et al., 1998; Fuglevand et al., 1993; Duchateau & Enoka, 2022; Caillet et al., 2023a). The smaller MUs usually attain higher discharge frequencies (De Luca & Hostage, 2010) and undergo a more rapid acceleration of the firing rate at recruitment and a more pronounced rate limiting than larger MUs (Lee and Heckman, 1998; Bennett et al., 1998; Binder et al., 2020; Avrillon et al., 2023a).

The neural drive to a muscle determines the force the muscle

* Corresponding authors.
E-mail addresses: l.modenese@unsw.edu.au (L. Modenese), d.farina@imperial.ac.uk (D. Farina).
[1] These authors have equal contributions and share the senior authorship.

https://doi.org/10.1016/j.jelekin.2024.102873

Available online 7 March 2024

produces. The muscle fibres build cellular force based on the frequency of discharged action potentials they receive from their innervating active MNs (Heckman & Enoka, 2004). The muscle aggregates the force-generating dynamics of the active MUs into a macroscopic pulling muscle force that is transmitted to the skeletal system. By modulating the recruitment and rate coding dynamics of the MN pool, the central nervous system voluntarily controls the muscle force (Milner-Brown et al., 1973; Van Cutsem et al., 1998; Enoka & Duchateau, 2017). Accurately estimating the neural drive to muscles allows for advanced neuromechanical investigations of the neural control strategy of muscle contraction and movement, thus advancing our understanding of how neural control signals are associated to muscle forces and behaviour (e.g., D'Avella & Bizzi, 2005; Powers & Binder, 2001; Hug et al., 2023, Powers & Heckman, 2017; Binder et al., 2020). In the establishment of human–machine interfacing, accurate estimations of the neural drive at MU-scale offer the possibility to directly exploit biological signals for the robust and intuitive control of assistive exoskeletons (Jung et al., 2021) and neuroprostheses (Farina et al., 2017; Farina et al., 2021). In clinical applications, the direct observation of the discharge activity of large populations of MUs finds applications in the diagnosis, monitoring and pathoetiological resolutions of neuromuscular disorders, such as spinal muscular atrophy (Kelly et al., 2023), amyotrophic lateral sclerosis (Bashford et al., 2020), and/or tremor (Puttaraksa et al., 2022), that primarily affect motor neurons and lead to an altered discharge activity of the MN pool, including changes in firing patterns, decreased MU recruitment, reduced MU action potentials amplitude, and increased fasciculations. Accurately estimating the neural drive to muscle in humans *in vivo* is however challenged by the difficulty of identifying the firing activity of full MU pools (Fig. 1, (Farina & Holobar, 2016; Avrillon et al., 2023a)), or of MU samples that are representative of the full MU pool (Fig. 1, first column).

This review presents modern electrophysiological and computational methods that allow us to accurately estimate the neural drive to muscle, i.e., the discharge activity of the full MU pool, at least in some muscles and in constrained laboratory conditions. First, we describe electrophysiological methods of surface and intramuscular high-density electromyography (EMG) acquisition and decomposition for identifying experimental samples of MUs that are representative of the full MU pool. The latter condition implies that a sufficient number of MUs is identified and that the identified MUs have recruitment thresholds that follow a physiological continuous exponential distribution, with more low-threshold units than high-threshold units (Fig. 1, second column). Then, we review computational methods of data augmentation that provide reliable estimates of the discharge activity of the full MU pool from limited experimental samples of discharging MUs (Fig. 1, third column). Finally, we apply these electrophysiological and computational methods to representatively demonstrate the accurate control of a MN-driven neuromuscular model of a MU pool.

2. Properties of MNs and MUs, and representative MU samples

It is currently not possible to experimentally detect the activity of full pools of active MUs in humans. Therefore, the neural drive to muscle is commonly inferred from limited samples of experimentally observed MUs. These samples must be representative of the active MU pool for accurate estimations of the neural drive. In this section, we will review the distribution of MN and MU properties across the pool, with special emphasis to their interrelations and their contribution to the neural drive. This discussion will be relevant to better specify the issue of representativeness of MU samples and to later explain how data

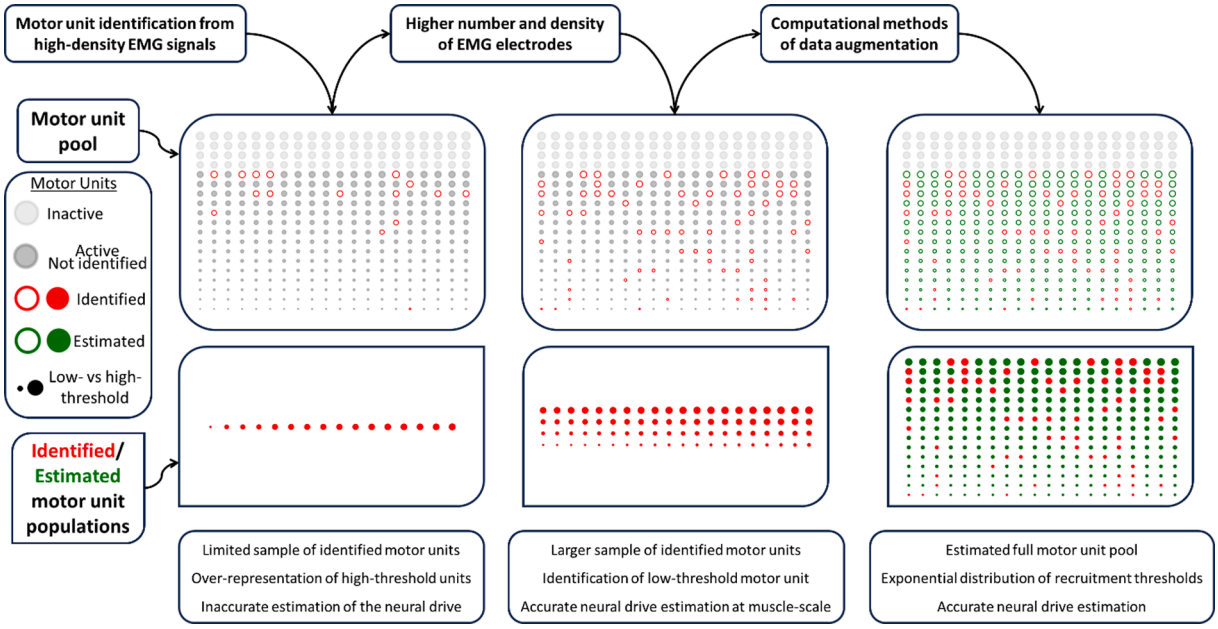

Fig. 1. Identification and estimation of the discharge activity of the active motor unit (MU) pool with electrophysiological and computational methods to estimate the neural drive to muscle in humans in *vivo*. The subplots in the first row display an exemplary pool of 400 MUs. Each MU is represented by a circle with a size schematically representing the MN size and therefore the MU's force recruitment threshold, following a physiological exponential distribution across the MU pool (given in Fig. 2). The MU population is here ranked from left to right and bottom to top in increasing order of recruitment thresholds. Here, 75% of the MU pool is recruited and 25% of the MUs are not active (first row: light grey circles). A sample of active MUs and their discharge activity (first row: red hollow circles; second row: plain red circles) can be identified in humans *in vivo* from the decomposition of high-density EMG signals. The MU samples commonly identified in this way (first column) are usually small and over-represent high-threshold MUs (large diameter circles). Therefore, these MU samples are usually not representative of the MU pool. Increasing the number and the density of EMG electrodes (second column) allows the identification of more MUs, especially low-threshold MUs, yielding MU samples that are more representative and that provide a more accurate estimation of the neural drive to muscle at the muscle-scale. Computational methods of data augmentation allow the estimation of the discharge behaviour of the MUs not identified experimentally (first two columns: dark grey plain circles, third column: green hollow and plain circles) and fully describe the neural drive to muscle. Adapted from data in the tibialis anterior muscle at 30% maximum voluntary contraction force by Caillet et al., (2023a,2023b).

augmentation methods can infer the activity of non-observed MUs from representative samples of observed ones.

2.1. The electrophysiological properties of a MN are inter-related

The input–output function of MNs, i.e., the transformation of net excitatory synaptic current into firing activity, is MN-specific. Indeed, the firing behaviour of a MN depends on its set of intrinsic electrophysiological properties. The MN-specific electrophysiological properties are inter-related with each other for each MN (Henneman, 1981; Burke, 1981; Binder et al., 1996; Powers & Binder, 2001; Kernell, 2006; Heckman & Enoka, 2012), as it can be quantified with mathematical equations that express each property as a function of the others (Table 4 in Caillet et al., (2022a)). According to these relations, the higher the value of current recruitment threshold in a MN, the greater the MN's global membrane capacitance and axonal conduction velocity, while the MN have smaller input resistance, afterhyperpolarization period, and membrane time constant. Besides, recent findings (Avrillon et al., 2023a) show that low-threshold MNs have a higher initial acceleration of firing rates, stronger rate limiting, and a more pronounced hysteresis than high-threshold MNs, because of MN-specific neuromodulatory inputs. Also, low-threshold MNs usually reach higher discharge rates than high-threshold MNs (onion-skin scheme (De Luca & Hostage, 2010)). Combined, these results indicate that the input–output function of MNs is MN-specific and each active MN contributes in a unique way to the neural drive to muscle.

2.2. MN and muscle fibre properties are correlated

The current recruitment threshold and force recruitment threshold of a MU are positively correlated, as indirectly demonstrated from separate measurements of current thresholds, torque recruitment thresholds, twitch torques, and tetanic forces in human and other mammal muscles (Heckman & Enoka, 2012; Caillet et al., 2022a). Furthermore, Caillet et al., (2022a) reported significant correlations between the tetanic force, twitch force, or innervation ratio of a MU and the axonal conduction velocity, input resistance, or current threshold of its innervating MN in cats and rodents. Therefore, the electrophysiological properties of a MN are also correlated with the properties of the muscle fibres it innervates. Notably, the early-recruited low-threshold (in current or force) MUs are activated at low forces before the higher-threshold (in current or force) MUs, that have large number of muscle fibres and therefore produce high forces. MN and MU properties are also quantitively correlated to MN and MU size (Caillet et al., 2022a), so that larger MNs and MUs have higher (current and force) recruitment thresholds (Henneman's size principle (Henneman, 1981)).

2.3. Distribution of MU thresholds

The inter-related properties of MNs and MUs are distributed continuously across the MU pool's recruitment range in mammals and do not cluster into discrete groups, as reviewed previously (Heckman & Enoka, 2012) and demonstrated with density histograms for several MN and MU properties (Caillet et al., 2022a; Duchateau & Enoka, 2022). Moreover, the force and current recruitment threshold properties of MUs are exponentially distributed (Fuglevand et al., 1993; Heckman & Enoka, 2012; Duchateau & Enoka, 2022; Caillet et al., 2022a), with many low-threshold MUs and few high-threshold MUs in the MU pool. Exponential distributions of force recruitment thresholds F^{th} were systematically observed in human muscles, including the human Tibialis Anterior (TA) (Feiereisen et al., 1997; Van Cutsem et al., 1998), masseter (Goldberg & Derfler, 1977), brachial biceps (Kukulka & Clamann, 1981), hand muscles such as the adductor pollicis (Kukulka & Clamann, 1981; Duchateau & Hainaut, 1990; Dengler et al., 1988) and first digital interosseous (Stephens & Usherwood, 1977; Dengler et al., 1988; Duchateau & Hainaut, 1990), and forearm muscles, such as the extensor carpi radialis (Romaiguère et al., 1989; Riek & Bawa, 1992) and extensor digitorum communis (Monster & Chan, 1977; Riek & Bawa, 1992). Of note, these studies might however report imprecise descriptions of the distribution of threshold properties across the full MU pool because they identified only a small fraction of the investigated MU pools (samples of 12 ± 10 MUs were identified per muscle and participant and merged, often without prior normalization, into sets of 81 ± 82 MUs for groups of 7 ± 9 participants). This limitation was recently addressed for the TA and Vastus Lateralis (VL) muscles (Avrillon et al., 2023a) when extensive samples of up to ~200 MUs were identified per muscle and subject over the full recruitment range (TA: 129 ± 44 MUs per participant, 895 MUs for 8 participants; VL: 130 ± 63 MUs per participant, 911 MUs for 8 participants). These extensive samples of unique MUs were obtained by iteratively tracking samples of identified MUs across eight contractions between 10 % MVC and 80 % MVC, which ensured identifying large MU samples for each recruitment range. The resulting distributions of force recruitment threshold F^{th} in the human TA and VL muscles are reported with density histograms and scatter plots in Fig. 2. They are, to the authors' knowledge, the most comprehensive descriptions of full MU pools currently proposed with electrophysiological methods for human muscles, and likely provide a reliable description of the full MU pool's distribution of threshold properties. From the scattered threshold distributions, continuous recruitment curves may be derived. As for the other investigated muscles (unpublished results based on the data provided in the afore-mentioned studies), the experimental F^{th} data points in Fig. 2 were better fitted with a linear-power relationship than with an exponential function, although the terminology 'exponential distribution of recruitment thresholds' is maintained in the following for simplicity. The fitted functions in Fig. 2 captured the threshold distribution with negligible error ($r^2 > 0.97$, $p < 0.001$, and 0.7 ± 0.8 % MVC absolute error in average across participants, up to 3.9 ± 2.8 % MVC absolute error for highest-threshold MUs and 1.9 ± 1.4 % MVC elsewhere). Smoothing the inherent variability in the measured MU recruitment thresholds with continuous fits is expected to have negligible effect on the methods discussed in this review, both in the assessment of representative MU samples and in the data augmentation methods discussed later. Indeed, in Fig. 2, the change in recruitment threshold value between consecutive MUs is negligible and adequately captured by a continuous function (0.4 ± 0.5 % MVC increase in average across participants, up to 1.2 ± 0.7 % MVC between the highest-threshold consecutive MUs and 0.8 ± 0.5 % MVC elsewhere). In fact, smoothing the scattered experimental measures may yield a more accurate description of the full pool, which samples the recruitment range with a higher numerosity of MUs than obtained experimentally and plotted in Fig. 2. Of note, ranking MUs by increasing recruitment thresholds disregards any recruitment dynamics diverging from the robust orderly recruitment scheme (Henneman, 1981), like task-specific mechanisms or reversal mechanisms occurring during rapid contractions (reviewed in Heckman & Enoka (2012)).

According to the cited literature and Fig. 2, MU recruitment curves are subject-specific. The distribution of MU recruitment thresholds is also muscle-specific and varies between muscles. For example, half of the MU pool is recruited below 10 % MVC in hand muscles (Duchateau & Enoka, 2022) against 25 % MVC in the TA and VL muscles (Fig. 2, (Enoka & Fuglevand, 2001)). Also, the recruitment range of MU pools is muscle-specific, as the MUs of hand, forearm, and lower limb or masseter muscles are recruited up to 30–35 % MVC (Duchateau & Hainaut, 1990), 50 % MVC (Kukulka & Clamann, 1981), and 70–90 % MVC (Fig. 2, (Goldberg & Derfler, 1977)), respectively. In conclusion, human muscles have more low-threshold MUs than high-threshold MUs, with a continuous exponential distribution of recruitment thresholds and in proportions that are subject- and muscle-specific. When assessing the representativity of a MU sample and its exponential distribution of thresholds, it is important to use for comparison recruitment curves from the same muscle or muscle group as the investigated MU pool to account

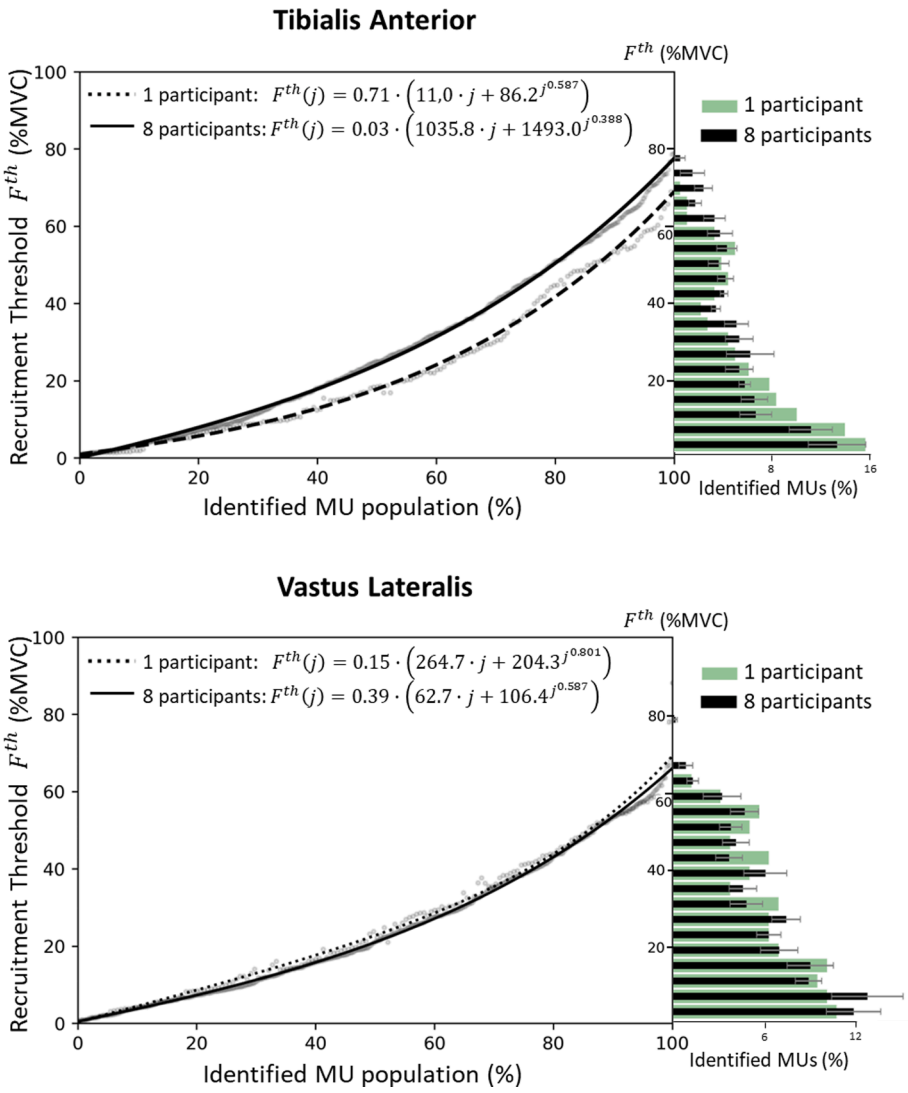

Fig. 2. Continuous distribution of motor unit (MU) force recruitment thresholds F^{th} across the MU pool of two human muscles. The experimental data was obtained by Avrillon et al., (2023a), where extensive samples of unique MUs (40–200 in a single participant, >800 for eight participants) were identified over a wide range of contraction intensities (10 % to 80 % MVC) for the tibialis anterior and vastus lateralis muscles. The density histograms report for a single participant (green bars) and for the cohort of eight participants (black bars) the percentage of identified MUs (x-axis) with respect to their measured force recruitment threshold F^{th} in percentage of the maximum voluntary contraction (%MVC) force (y-axis). Grey error bars report the dispersion between participants (one standard deviation). Bins are 4 % MVC-wide. An exponential distribution is observed; many MUs have low recruitment thresholds and few MUs have high recruitment thresholds. The scatter plots report for a single participant (light grey data points) and for the cohort of eight participants (black bars, dark grey data points) the relationship between the force recruitment threshold F^{th} (in %MVC, y-axis) of a MU and the rank (in %, x-axis) it occupies in the identified MU pool, ranked in ascending order of recruitment thresholds. The clouds of data points were fitted with the linear-power relationships ($r^2 > 0.97$, $p < 0.001$) of the form $f(j) = a \bullet \left(b \bullet j + c^{j^d}\right)$, where $j \in [0;1]$ (the scale of the x-axis, in percentage, is then 100 • j %). The fitted relationships are reported for information in the inset and estimate the percentage of the MU population recruited at a certain recruitment threshold. The parameters a,b,c, and d respectively control the scaling, the slope of the linear part, the rate of exponential increase, and the rate of change of the exponential growth of the function. Linear-power relationships returned better fits than purely exponential and linear-exponential functions. However, the terminology 'exponential distribution of recruitment thresholds' is used in this study for clarity. The relationships are reported in the normalized space ($j \in [0;1]$) because of the high uncertainty in the number N of MUs in human muscles. In a pool of N MUs, these relationships can be adapted with the $j \rightarrow \frac{j}{N}$ transformation, where j becomes an integer in $[\![1;N]\!]$. The results presented here are, to the authors' knowledge, the most detailed available descriptions of the MU threshold distribution in the TA and VL muscles and provide a credible description of the yet not fully decoded full MU pool. These results serve in the following for assessing whether MU samples follow the muscle-specific exponential distribution of the full pool. It is worth noting that joint torques were measured in Avrillon et al., (2023a); in these experiments, the ankle and knee joint torques normalized to the measured maximum voluntary torques are acceptable indicators of the tibialis anterior and vastus lateralis muscle forces in percentage of their maximum physiological forces, respectively, hence the terminology 'Force recruitment thresholds' in %MVC taken here. Indeed, the bipolar EMG signals concurrently recorded from the co-contracting agonist and antagonistic muscles did not show significant changes in relative activation across contraction intensities (Avrillon et al., 2023a), while the net joint torque produced by co-contracting agonist and antagonistic muscles remained constant across torque intensities, as calculated and confirmed by EMG-driven musculoskeletal estimations of the forces developed by those muscles (see Caillet et al., (2023a) for details on the taken EMG-driven musculoskeletal approach).

for the muscle-specificity of threshold distributions.

2.4. Representative samples of MUs

As a practical definition, a MU sample is representative of the MU pool if the activity of the MUs of the sample retains most of the information contained in the activity of the full pool of MUs. This implies that a representative sample should be "sufficiently" large and with a distribution of recruitment thresholds similar to that of the full pool, i.e., continuous and approximately exponential. The conditions on size and continuity are needed to avoid gaps in MU behaviour in specific recruitment force ranges. Because of the need to represent an exponential distribution, a sample of MUs is representative of the full MU pool if it contains many more low-threshold than high-threshold MUs. The threshold distribution of the MU sample may be compared to a ground-truth distribution for the full pool, like the density histograms in Fig. 2, with a Bhattacharyya coefficient D_B (Bhattacharyya, 1943) (0: no similarity; 1: complete overlap between distributions).

In the following example, we describe a representative sample of MUs for a human TA muscle contracting at 50 % of the maximum voluntary contraction (MVC) force. According to recent reviews (Caillet et al., 2022b; Duchateau and Enoka, 2022) and to the lower bound of 199 identified MUs reported in (Avrillon et al., 2023a), the TA muscle may comprise a potentially conservative total of N = 400 MUs (reported range: 122–550 MUs). The estimated N = 400 MUs scale the normalized TA-specific recruitment curve in Fig. 2 (top plot) with the transformation $j \rightarrow \frac{j}{N}$, where $j \in [0;1] \rightarrow [\![1;N]\!]$. The scaled recruitment curve yields that approximately 320 MUs are recruited at 50 % of the MVC force. In these conditions, a sample of 32 MUs (i.e., 10 % of the active pool) would be representative of the MU pool ($D_B = 1$) if 10, 7, 6, 5, and 4 MUs were identified for each 10 %-MVC interval of force, as given by the F^{th}-distribution of the full MU pool (solid curve) in Fig. 2. It is worth noting that the estimated N = 400 and more globally Motor Unit Number Estimation (MUNE) techniques, which have been applied to few human muscles for which inter-subject variability is scarcely discussed, are associated with substantial uncertainty because of specific limitations associated with current MUNE techniques, such as cadaveric analyses, statistical methods, spike-triggered-averaging approaches, and adapted multiple point stimulation.

3. Estimation of the neural drive to muscle

It is currently not possible to directly observe during a motor task all concurrently active MUs of a human muscle. Conversely, the neural drive to muscles can be indirectly approximated by electrophysiological features associated to its intensity, such as the amplitude of EMG signals, or from experimental samples of observed MU activities.

3.1. Global analysis of EMG signals

The neural drive to muscles has been classically approximated from the myoelectric activity detected with electrodes applied on the skin covering the investigated muscle (surface EMG) or inserted into the muscle (intramuscular EMG) (Besomi et al., 2019; De Luca, 1997; Farina et al., 2004). In this context, recent tutorials (Merletti & Muceli, 2019; Merletti & Cerone, 2020; Clancy et al., 2023) and consensus studies (Besomi et al., 2020; Gallina et al., 2022) provide best practices for optimal choice of electrode design, montage, and placement, and for optimal EMG acquisition and post-processing. For example, the estimate of amplitude of the surface EMG, e.g., low-pass filtered rectified EMG, is commonly associated to the intensity of the neural drive to muscle (Farina et al., 2014b). However, EMG amplitude provides only a crude description of the neural drive. Indeed, surface EMG signals are influenced by the volume conductor properties as well as by amplitude cancellation, i.e., the amplitude of the interference EMG signal is less than the sum of the amplitudes of the MUAP trains (Farina et al., 2014b). The amount of amplitude cancellation differs between MUs and is greatest for small surface-recorded action potentials, which are associated with low-threshold small MUs and MUs located far from the recording electrodes. Consequently, amplitude cancellation reduces the contribution of some MUs to the estimate of EMG amplitude and the magnitude of the deficit cannot be predicted or compensated (Farina et al., 2014b). Also, the contribution of the discharging MUs to the EMG signal amplitude is determined by the amplitude of their MUAPs as filtered by the volume conductor and detected by the electrodes. Consequently, the large MUs that include many fibres and the MUs that are superficial and located close to the recording electrodes are over-represented in the recorded EMG signals. Conversely, surface EMG amplitude can be relatively insensitive to changes in the activity of small low-threshold MUs or MUs located far from the recording electrodes, i.e., deep MUs. For these reasons, the amplitude of surface EMG signals provides a relatively poor estimate of the intensity of the neural drive to muscle (Farina et al., 2014b). Estimates of the neural drive from the global analysis of EMG signals are sufficient in some applications but not in others, for example when building accurate subject-specific neuromusculoskeletal models of a motor task (Lloyd et al., 2023).

3.2. Samples of identified MUs from decomposed high-density EMG signals

The combination of arrays of high-density EMG (HDEMG) electrodes with modern source-separation algorithms enables the identification of MU discharges in human *in vivo* (Holobar & Farina, 2014; Negro et al., 2016; Farina & Holobar, 2016). Contrary to the global analysis of EMG signals, samples of identified MUs provide a direct information on the discharge dynamics of the decoded MU population, which is a first step towards the identification of the neural drive to muscle. In brief, source-separation methods identify spike trains specific to individual MUs from the multi-unit EMG based on their characteristic MUAP shapes. Beside source separation methods, other approaches have been proposed to decompose the EMG signal, such as based on the detection of templates of MUAP waveforms (De Luca et al., 2006; Nawab and Luca, 2010). Consensus studies (Hug et al., 2021a; Gallina et al., 2022; Martinez-Valdes et al., 2023), tutorials (Del Vecchio et al., 2020; Avrillon et al., 2023b), open-source tools (Avrillon et al., 2023b; Valli et al., 2024) and commercial software packages (e.g., DEMUSE: https://demuse.feri.um.si/) for HDEMG acquisition, decomposition and/or spike train editing are available, with ongoing research towards fully automated methods for spike train identification (Clarke et al., 2020; Rossato et al., 2023).

3.3. Classic limitations of EMG decomposition

Current source-separation algorithms tend to identify the MUs with the largest MUAPs within the EMG signal (Farina & Holobar, 2016). As high-threshold MUs have the largest innervation ratios in the MU pool (see Fig. 2 in Caillet et al., (2023a)), decomposition techniques tend to favour the identification of the higher-threshold MUs. Therefore, by usually over-representing high-threshold over low-threshold MUs, the identified MU samples are likely not representative of the MU pool, as they do not follow an exponential distribution of recruitment thresholds (i.e., a greater proportion of low-threshold MUs over high-threshold MUs). In addition to this bias, it is usually difficult to identify large samples of MUs. With surface grids of 64 electrodes and/or intramuscular arrays of 40 electrodes, high-yield decomposition typically identifies samples of 5–40 MUs per muscle per contraction (Del Vecchio et al., 2020; Hug et al., 2021b; Muceli et al., 2022). This is still a limited portion of the MUs in human muscles that are typically hundreds to a few thousands. For these reasons, it is challenging to identify, with current EMG recording and decomposition techniques, MU samples that accurately estimate the neural drive to muscle (Fig. 1, first column). For example, Caillet et al., 2022b computed the neural drive at the muscle-

scale with publicly available datasets of few identified MUs (i.e., 14–32 MUs), that over-represent higher-threshold with respect to lower-threshold MUs. The predicted neural drive, that was calculated as the low-pass filtered (10 Hz) cumulative spike train and validated against the normalized recorded joint torque as previously proposed (Farina & Negro, 2015), substantially underestimated the true neural drive in the regions of low forces. Solutions to this problem are discussed in the following.

3.4. Dense surface EMG grids of electrodes

Increasing the density and number of surface EMG electrodes yields larger and more representative samples of identified MUs (Fig. 1, second column). Specifically, dense grids of surface EMG electrodes allow to better identify low-threshold MUs, while increasing the number of surface EMG electrodes allows to identify greater number of MUs. This was recently demonstrated by Caillet et al., (2023b), who showed decomposition of EMG signals recorded from the TA muscle with surface grids of 256 electrodes and 4-mm interelectrode distance (IED), as well as six grids of lower size, electrode density, and number of electrodes. The conclusions on electrode number and density were confirmed with computational simulations and with an ultra-dense grid of 2-mm IED in the same study (Caillet et al., 2023b), as well as for the VL muscle (unpublished results obtained from the publicly available data by Avrillon et al. (2023a)). Fig. 3 reports the density histograms (blue bars) of the MUs identified with three grids of 4-, 8-, and 12-mm IED and 256, 64, and 35 electrodes.

Increasing the electrode density gradually revealed early-recruited MUs that were not identified with lower-density grids. For example, up to 32 % (range: 6–44 %) of the MUs identified with the densest grid (256 electrodes, 4-mm IED) were early-recruited MUs (i.e., in the first half of the active MU pool), against only 11 % (range: 0–24 %) when using grids of 12-mm IED. Importantly, relatively more early-recruited MUs were identified than late-recruited MUs when increasing electrode densities. Increasing the total number of electrodes, either by increasing the grid size or electrode density, gradually revealed MUs that were not identified with fewer electrodes. Notably, the number of identified MUs doubled with 256 electrodes (4-mm IED and 36 cm^2) against 64 electrodes (4-mm IED or 8-mm IED), reaching 56 ± 14 MUs and 45 ± 10 MUs for contractions up to 30 % and 50 % MVC, respectively.

Increasing the electrode density, the size of the grid, and/or the number of electrodes improved the spatial sampling (e.g., IED < 5 mm to avoid spatial aliasing (Afsharipour et al., 2019)) of the action potential waveforms. As a consequence, the pulse-to-noise ratio of the spike trains of the small MUs and MUs far from the recording sites increased, better separating sources from the additive noise in the mixture model of the EMG signal and enabling their accurate identification (Caillet et al.,

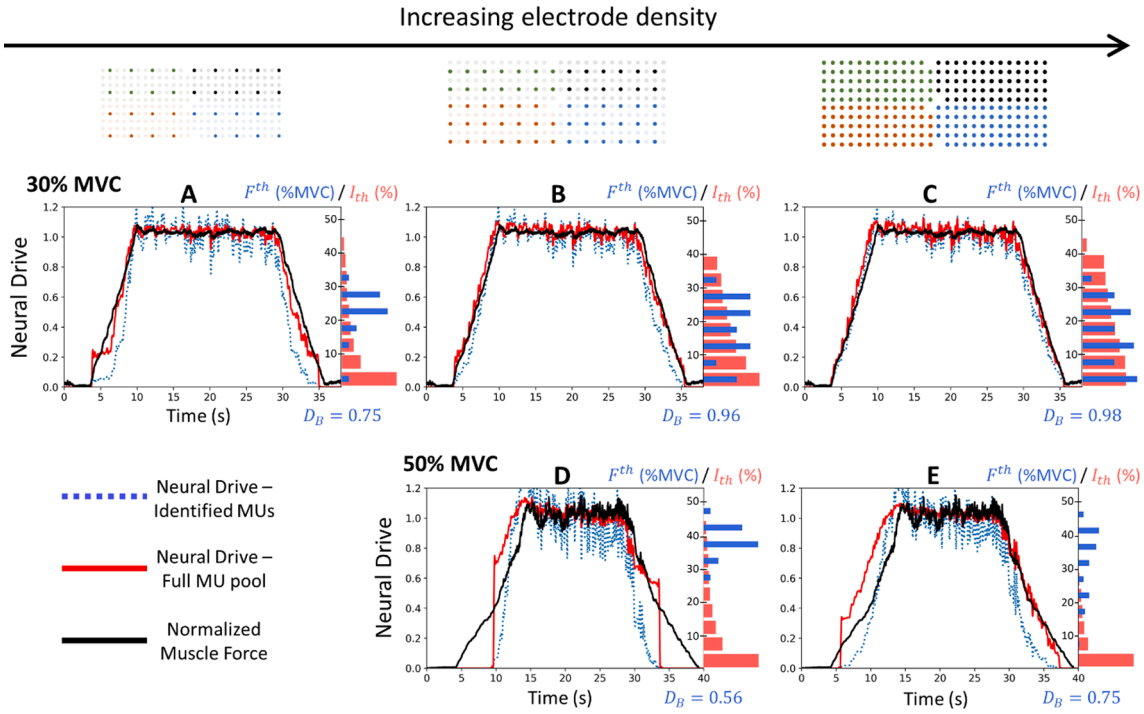

Fig. 3. Estimation of the neural drive to muscle from populations of discharging motor units (MUs). The data and results were obtained in Caillet et al., (2023a,2023b). EMG signals were recorded from the tibialis anterior muscle with three grid configurations of increasing electrode density (from left to right: grids of 12-mm, 8-mm, and 4-mm interelectrode distance involving 35, 64, and 256 electrodes, respectively) during trapezoidal contractions up to 30 % maximum voluntary contraction (MVC) (first row) and 50 % MVC (second row). Samples of MUs were identified from the decomposition of these EMG signals. The histograms report the density distribution of the MUs across the recruitment range in 5 %-steps. The distribution of experimentally-identified MUs is reported with blue bars according to their measured force recruitment thresholds F^{th} (in %MVC). The similarity of these experimental threshold distributions with the ground-truth distribution given in Fig. 2 is assessed with the calculation of the Bhattacharyya coefficient D_B in [0; 1]. $D_B = 1$ suggests that the MU sample is representative of the exponential distribution of thresholds of the full MU pool. The distribution of the reconstructed MU pool is reported with red bars according to the MUs' current recruitment thresholds (rheobase) I_{th} (in percentage of the maximum theoretical value for I_{th}). Here, I_{th} is predicted from the MN size S, that is estimated by the data augmentation method (see next section for details) as $I_{th} = 3.8 \bullet 10^8 \bullet S^{2.52}$ (Caillet et al., 2022a). The histograms were normalized to the total number of MUs in each configuration. The experimental neural drive was estimated from the samples of identified MUs (dotted blue traces, Neural Drive – Identified MUs). The neural drive was also estimated from the discharge activity of the artificial full pool population of $N = 400$ MUs (solid red traces, Neural Drive – Full MU pool), that was generated from the experimental MU samples with computational methods (Caillet et al., 2022b) (see next section for details). In all cases, the neural drive was obtained by summing the binary spike trains of the available MUs and low-pass filtering the resulting cumulative spike train. The resulting neural drives (in arbitrary units) were normalized to the average computed value over the plateau of force (Caillet et al., 2023a, 2023b). The normalized neural drives were validated in the normalized space against the measured TA force (Farina & Negro, 2015; Enoka & Farina, 2021) (solid dark trace, see text for details on the validation).

2023b). It is worth noting that the beneficial effects of high spatial sampling and the rate at which additional MUs were detected with higher number of electrodes decreased when the grids became very dense (<4-mm IED), in which case the MUAPs detected by adjacent electrodes were highly correlated (coefficient of correlation of 0.98 at 2-mm IED) (Caillet et al., 2023b).

As a result, the densest grids of electrodes returned samples of identified MUs that spanned across the complete recruitment range, approaching the physiological exponential distribution of recruitment thresholds necessary for accurate neural drive estimation (see top-middle and top-right density histograms in Fig. 3, blue bars). Conversely, the grid with 12-mm IED revealed few of the active low-threshold MUs recruited during the first half of the muscle contraction. Moreover, increasing the number of electrodes helped identifying MUs for each interval of recruitment thresholds. Therefore, the MU samples derived with higher electrode density and number of electrodes were more representative of the full pool, with systematically increasing Bhattacharyya coefficients D_B between the threshold distributions of the full pool (estimated in Fig. 2) and of the MU sample (see Fig. 3). The neural drive to muscle was consequently better estimated, as displayed in Fig. 3 and demonstrated by Caillet et al., (2023a). For example, the low-density grid of 35 electrodes returned an inaccurate estimate of the neural drive (top-left subplot in Fig. 3) with sudden jumps and drops over the interval of recruitment threshold where no MUs were identified, and underestimation in the regions of low forces where the low-threshold active MUs were not identified. Conversely, more accurate estimates of the neural drive were obtained with the dense grid of 256 electrodes (top-right subplot in Fig. 3).

3.5. Dense intramuscular EMG arrays of electrodes

High-density arrays of intramuscular electrodes based on thin-film technology have also been proposed (Muceli et al., 2015, 2022; Chung et al., 2023). Like surface EMG, the number of identified MUs increases with the number of intramuscular recording sites. Negro et al. (2016) automatically decoded 20 ± 3 (up to 24) MUs in the TA muscle from 16 to 32 intramuscular recording sites at forces ranging from 10 to 30 % MVC, while Muceli et al. (2022) automatically decoded 31 ± 5 (up to 40) MUs when using 40 channels at 30 % MVC, and up to 67 MUs with 80 channels. Source-separation algorithms might detect relatively more low-threshold MUs from intramuscular EMG than surface EMG, as intramuscular EMG is not subject to the filtering and attenuating effects of the subcutaneous and skin layers and has higher signal-to-noise ratio than surface EMG (Besomi et al., 2019). It remains to be investigated whether the MU samples identified with intramuscular high-density arrays of electrodes are representative of the full MU pool. Importantly, intramuscular arrays of electrodes can identify the activity of the deep MUs that cannot be detected from surface EMG. Measurements may therefore combine surface and intramuscular arrays of electrodes to detect separate MU populations in difference portions of the muscle (Muceli et al., 2015). Therefore, concurrently recording EMG signals from dense and large surface grids of electrodes and multiple intramuscular high-density arrays of electrodes targeting different populations of deep MUs can increase the experimental yield of MUs and the identification of a strongly representative sample of the MU pool (Negro et al., 2016; Muceli et al., 2022).

3.6. Selecting optimal subsets of the identified MUs

While it is possible with modern approaches to increase the number of experimentally identified MUs and favour to some extent the identification of low-threshold MUs, as discussed above, the distributions of these experimental samples are rarely matching the muscle-specific exponential distribution of MUs in the full pool (D_B coefficient systematically below 1.0 in Fig. 3). It is possible to select optimal subsets of the identified MUs to match the full pool distribution. To do so, we are using the threshold distributions in Fig. 2 as ground-truth representations of full MU pools. As a reminder, these distributions were derived from extensive populations of identified MUs but are associated with a certain degree of uncertainty, considering that the full pool was not decoded. According to Fig. 2, a TA muscle contracting at 30 % MVC has a third of its active MUs recruited below 8 % MVC, another third between 8 and 18 % MVC, and another third between 18 and 30 %MVC (Fig. 2), i.e., following a 33 %–33 %-34 % split of the pool of active MUs over these three 0–8, 8–17, and 17–30 % MVC recruitment ranges. Conversely, the 64-electrode grid returned, for the group of participants in Caillet et al., (2023b), a 10 ± 5 % − 26 ± 10 % − 64 ± 10 % split of identified MUs over those three recruitment ranges. This indicates that the higher-threshold MUs in the 18–30 % MVC range are over-represented. As expected, the 256-electrode grid returned a more balanced 16 ± 9 % − 26 ± 8 % − 58 ± 16 % split, although the higher-threshold MUs were still over-represented (Caillet et al., 2023b). To address this limitation, it is possible to select an optimal MU subset of the identified MU sample, that is more representative of the MU pool, by discarding some of the identified MUs that fall into the recruitment threshold ranges that are over-represented. The selected optimal subsets would better estimate the neural drive to muscle than the original samples of identified MUs. This approach by optimal subsets proved beneficial in dexterous human–machine interfacing (Yeung et al., 2023), for example.

To illustrate this approach, we analysed here 500,000 random combinations of subsets of the MU samples identified in Caillet et al., (2023b), without repetitions within and between subsets, and with more than 15 MUs. The 200 combinations of MUs that best estimated the neural drive at muscle-scale (according to a weighted combination of normalized coefficient of determination and root-mean square error) were extracted. On average, the optimal subsets of MUs followed a 25 ± 2 % − 29 ± 3 % − 46 ± 3 % distribution over the three defined recruitment ranges, when the original MU sample was obtained with the 256-electrode grid. A similar 23 ± 3 % − 30 ± 2 % − 49 ± 4 % split was achieved by the optimal subsets of the 64-electrode grid. In one participant, for whom many low-threshold MUs were identified (top-right quadrant in Fig. 3), the optimal subset achieved a close-to-theoretical 30 %–32 %-38 % split. Those optimal subsets (closer to the theoretical 33 %–33 %-34 % split than original samples) better estimated the neural drive to muscle than the original MU samples by effectively discarding a portion of the over-represented higher-threshold MUs and retaining the identified lower-threshold MUs. This method by optimal subsets however reduces the available experimental data and impoverishes our direct experimental observation and understanding of the dynamics of neural control strategy in humans *in vivo*. The discarded experimental data may rather be used to infer the activity of the non-identified active MUs, as we will discuss later.

3.7. Limitations of state-of-the-art recording and decoding methods

Despite the recent improvement discussed above, experimental approaches for the identification of representative samples of MUs still present several limitations. First, experimental MU decoding is mainly limited to isometric and static contractions but other force trajectories more representative of daily-life contractions should be investigated. New computational approaches are emerging to address challenges related to muscle-grid shift and changes in muscle geometry that affect the spatial sampling of the MUAP waveforms and identify individual MUs in quasi-static (Oliveira & Negro, 2021) and dynamic (Glaser & Holobar, 2018; Kapelner et al., 2019; Yokoyama et al., 2021) tasks. Second, the identification of many low-threshold MUs is not always possible. For example, very few low-threshold MUs were identified in Caillet et al., (2023b) during high-force contractions, even with the densest grids of electrodes (similar results are obtained at high forces by the intramuscular dense arrays). Consequently, inaccurate estimations of the neural drive were obtained for high-force contractions, irrespective of the electrode density, in the regions of low forces where very

few low-threshold MUs were identified (Fig. 3, bottom row). The percentage of identified low-threshold MUs is also highly subject-specific, with a high disparity of results reported between subjects (Caillet et al., 2023b). It is likely muscle-specific, although no significant difference was found between the TA and VL muscles (Avrillon et al., 2023a), and gender-specific, as fewer low-threshold MUs are usually identified in females than males using non-invasive methods (Jenz et al., 2023). To ensure the identification of many MUs over the full recruitment range, one can track identified MUs across multiple contraction intensities. For example, Avrillon et al. (2023a) applied this method with the 256-electrode montage over the TA (VL) muscle of 16 participants for eight contractions between 10 % MVC and 80 % MVC, and identified samples of 129 ± 44 (130 ± 63) unique MUs per subject and muscle, the density distribution of which displayed the physiological exponential tendency (black bars in Fig. 2) typical of the full MU pool.

4. Computational augmentation of experimental MU samples

Although MUs can be identified over the full recruitment range in some conditions, including many low-threshold MUs and approaching representative depictions of the full pool (Fig. 3B, C), it remains impossible to experimentally detect the activity of full pools of active MUs, i.e., to experimentally identify the neural drive at the MU scale. To address this limitation, computational methods of data augmentation (Caillet et al., 2022b; Ornelas-Kobayashi et al., 2023) have been recently developed to derive reliable estimates of the discharge activity of the full MU pool from a limited sample of identified MUs (Fig. 1, third column). An open-source implementation of the approach proposed by Caillet et al., 2022b is publicly available at https://github.com/ArnaultCAILLET/Caillet-et-al-2022-PLOS_Comput_Biol.

4.1. Methods of experimental data augmentation

Caillet et al., 2022b proposed a computational data-driven method

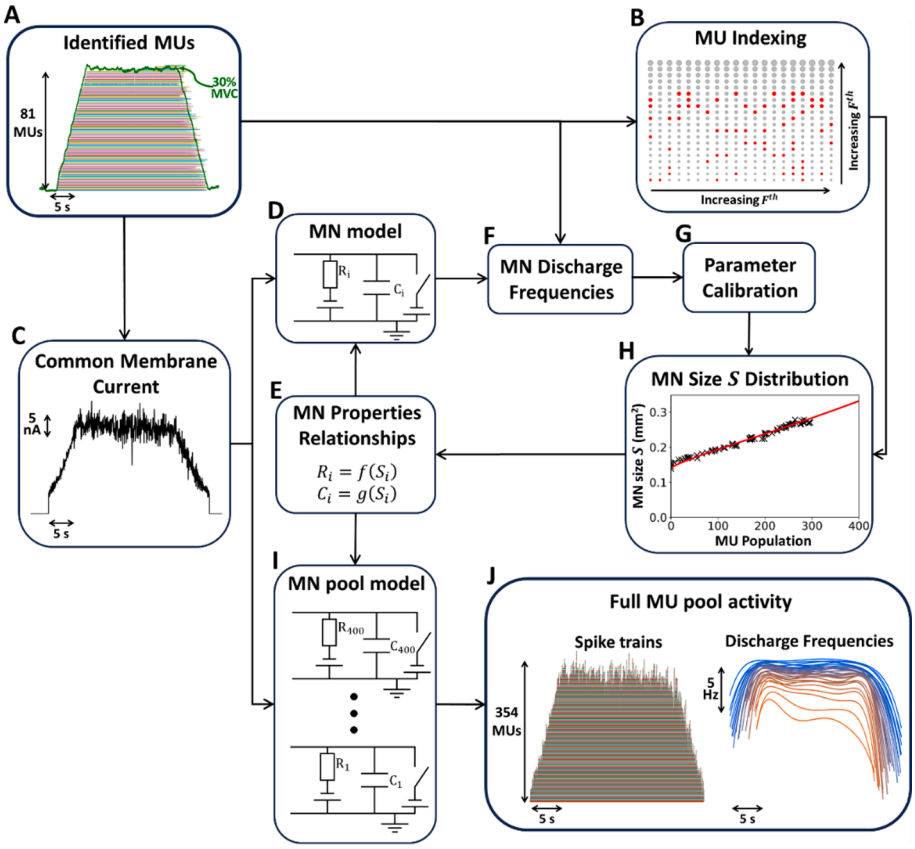

Fig. 4. Computational method for reconstructing the discharge activity of the full pool of motor units (MUs) from a limited sample of experimentally-identified MUs (Caillet et al., 2022b). (A) In this example, the spike trains of 81 MUs were identified from the decomposition of high-density EMG signals (256 electrodes, 4-mm interelectrode distance, 36 cm^2, see Fig. 3) recorded during a trapezoidal isometric contraction of the tibialis anterior muscle up to 30 % maximum voluntary contraction (MVC). (B) The 81 identified MUs (red circles) are mapped with an index $i \in [\![1;N]\!]$ into the MU pool of $N = 400$ MUs, fully schematized here, according to their measured force recruitment threshold F^{th}. The grey circles denote MUs that were not identified experimentally. The exponential increase of the MUs' force recruitment thresholds F^{th} across the MU pool (given in Fig. 2) is schematically represented from left to right and bottom to top by circles of increasing diameters. (C) The MN Common Membrane Current, common to all modelled MNs, is derived from the Common Synaptic Input to the MU pool following a procedure detailed in main text. The Common Synaptic Input is inferred from the discharge activity of the 81 identified MUs. (D) The Common Synaptic Input drives a revisited leaky-integrate-and-fire model of motoneuron (MN), the electrophysiological properties (e.g., input resistance R, membrane capacitance C) of which are all mathematically related to the size of the MN S, i.e., the total MN membrane surface area, according to a framework of mathematical relationships between interrelated MN-specific properties derived elsewhere (Caillet et al., 2022a) and discussed in Section 2.1. (F) For each of the 81 identified MUs, the MN firing behaviour is predicted by the LIF model and the difference between model-predicted and experimental MN discharge frequencies is minimized by (G) calibrating the MN-specific size parameter S. (H) The discrete S-distribution is fitted, resulting in a continuous distribution for the S parameter. The resulting continuous distribution of MN-specific electrophysiological properties (E) scales a pool of $N = 400$ MN models (I), that transforms the Common Synaptic Input (C) into the discharge activity of the full MU pool (J). It is worth noting that the method presented here, which considers a single common input driving a group of MNs, may be extended to multiple groups of MNs (e.g., MN clusters in a MN pool (Hug et al., 2023)), modelled as separate cohorts of MN LIF models and receiving specific common membrane currents that would be estimated separately.

that uses the physiological information of a sample of identified MUs to computationally estimate realistic discharge activities (i.e., spike trains) for the remaining non-identified MUs. This method is briefly described in the following and is applied in Fig. 4 with an input sample of 81 MUs identified from surface HDEMG signals (Fig. 4A).

The experimentally identified MUs are first indexed ($i \in [\![1; N]\!]$) in the full pool of N MUs, according to their recorded recruitment threshold value F^{th} and a typical muscle-specific F^{th}-distribution across the MU pool (e.g., Fig. 2). Then, the common drive responsible for the discharge activity of the identified MUs is estimated (Fig. 4C). To do so, the neural drive is first computed from the experimental spike trains (as the low-pass filtered cumulative spike train) and is then linearly associated to the common synaptic input (i.e., the net excitatory synaptic influx common to the MN population) in arbitrary values (Farina & Negro, 2015). The single-compartment LIF models with current synapses used in Caillet et al. (2022b) do not describe the nonlinear transformation of common synaptic input into dendritic activity. Therefore, as a modelling simplification, the total dendritic membrane current responsible for spike generation was directly piecewise-linearly scaled from the common synaptic input with physiological values of MN current recruitment threshold, taken from Caillet et al., (2022a). Some physiological dynamics resulting from the missing nonlinear transformation, such as the firing rate saturation, were captured by phenomenological parameters added to the LIF model. To stress this modelling simplification and avoid confusion, the total dendritic membrane current hence modelled was renamed 'Common Membrane Current' (in nanoAmpere, Fig. 4C). Then, the method determines, for each identified MU, the set of MN-specific electrophysiological properties that best explain its observed discharge activity. These properties (i.e., membrane time constant, input resistance, current recruitment threshold) are the parameters of a single-compartment leaky-integrate-and-fire (LIF) model of the MN (Fig. 4D). Those inter-related properties are entirely determined by the MN size parameter S, i.e., the total MN membrane surface area, as direct result from the discussion in Section 2.1 about the mathematical inter-relation between MN properties (Fig. 4E, (Caillet et al., 2022a)). The calibrated LIF model transforms the Common Membrane Current (Fig. 4C) into a train of discharge events. After calibration of the size parameter S (Fig. 4G), the MN-specific LIF model minimizes the root-mean-square difference between experimental and LIF-predicted filtered discharge frequencies (Fig. 4F). Next, the scatted pairs $\{i; S_i\}$ (black crosses in Fig. 4H) of MN index i (Fig. 4B) and calibrated parameter S_i (Fig. 4D-G) are fitted with a continuous function (red solid trace in Fig. 4H). The resulting S-distribution, to which the previously-introduced mathematical relationships are re-applied (Fig. 4E), determines the continuous distributions across the MU pool's recruitment range of the MN electrophysiological parameters of the LIF model. Finally, the discharge activity of the full pool of active MUs is predicted. A population of N LIF models of MNs (Fig. 4I) is scaled with the continuous distributions of MN-specific electrophysiological properties derived in the last step. The digital twin of the full pool of N MUs transforms the Common Membrane Current into a physiologically plausible estimation of the discharge activity of the full pool of active MUs (Fig. 4J).

Ornelas-Kobayashi et al. (2023) proposed a computational method similar in some steps to that of Caillet et al., 2022b, applied to a 15-parameter single-compartment conductance-based model with four ion-gating channel types (Cisi & Kohn, 2008). This model of MN is more physiologically accurate than the LIF model shown in Fig. 4D, however it is substantially more complex. As ion-gating channel-related parameters are difficult to measure in mammals (Bondarenko et al., 2004; Fohlmeister, 2009), Ornelas-Kobayashi et al. (2023) kept 12 MN parameters generic and constant, as in the original model (Cisi & Kohn, 2008), and identified the three remaining parameters with separate calibration routines. Consequently, the sets of MN parameters were not inter-related and were only partially MN-specific in that study, contrary to those derived in Fig. 4. Conversely, when MN-specific parameters are inter-related (like in Fig. 4E), a single calibration procedure is sufficient for accurate MN-specific predictions.

In conclusion, depending on the objective of the study, a trade-off must be found on MN model complexity. When reconstructing the full MU pool for estimating the neural drive to muscle, reconstructing the comprehensive exponential distribution of the MU recruitment thresholds is of critical importance, as achieved in Caillet et al., 2022b (red bar histograms in Fig. 3). Conversely, in Ornelas-Kobayashi et al. (2023), the trapezoidal contractions of very short ramps, where all active MUs are recruited over short 0.5-to-2-second periods, prevent from investigating the recruitment activity of the MU pool and are unfit to assess the distribution of the reconstructed full pool of MUs across the recruitment range. In many applications, detailing the physiological mechanisms responsible for firing action potentials is not necessary, as long as the predicted spike trains are accurate. In such cases, the flexibility of simple LIF models for receiving distributions of MN-specific inter-related MN parameters (Fig. 4D,E) is more suitable for accurately reconstructing the MU pool activity, while additional MN modelling complexity is not warranted and may become a limiting factor due to the increased number of independent parameters to identify via optimization approaches.

The two reconstruction methods described above are currently the only methods in the literature that drive a computational model of MN pool with motoneuronal data that is obtained experimentally. MN pool models of varying complexity were previously proposed (Fuglevand et al., 1993; Cisi & Kohn, 2008; Dideriksen et al., 2010; Dideriksen et al., 2011; Negro & Farina, 2011; Watanabe et al., 2013; Farina et al., 2014a; Potvin & Fuglevand, 2017), although they were tested and driven with artificial inputs, inputs from interneurons, or feedback systems.

4.2. Estimation of the neural drive to muscle

The full pool of artificial MUs obtained with the reconstruction method summarised in Fig. 4 (Caillet et al., 2022b) always provides a more accurate estimate of the neural drive at the muscle-scale than the original experimental sample of identified MUs (red solid traces versus blue dotted traces in Fig. 3). This was demonstrated with 23 MU samples identified from EMG signals recorded from the TA and VL muscles with grids of varying electrode densities in eleven subjects performing trapezoidal contraction forces at up to 30 % and 50 % MVC ((Caillet, 2023) and unpublished results obtained from the publicly available data by Avrillon et al. (2023a)). The higher accuracy in estimating the neural drive at muscle-scale is partially explained by the exponential distribution of recruitment thresholds obtained for the full pool of N artificial MUs (histograms of Fig. 3, red bars). Of note, the predicted quasi-linear S-distribution shown in Fig. 4H nonlinearly transforms into an exponential distribution of current recruitment thresholds I_{th} with the mathematical relationship $I_{th} \propto S^{2.52}$ (Caillet et al., 2022a).

The full pool of artificial MUs provides a comprehensive description of the neural drive at the MU-scale, by estimating the discharge activity for each active MU of the pool. The pool of artificial MUs is a realistic digital twin of the full pool of MUs when the chosen value of N (MU pool size) is of the same order of magnitude as the MUNE value for the investigated muscle, despite its substantial uncertainty as discussed previously. Importantly, the estimates of MU discharge activity are accurate; this was demonstrated with a leave-one-out cross-validation (i.e., each data point is sequentially held out as a validation set while the remaining data is used for training, assessing the model's generalization performance) that confirmed the accuracy of the estimated discharge activity for each of the identified MUs (Caillet et al., 2022b). Moreover, the discharge activity of the reconstructed pool is compatible with other physiological laws like the onion-skin strategy (De Luca & Hostage, 2010) (Fig. 4J), regardless of the quality of the input MU sample. This accuracy in replicating physiological dynamics is achieved because the method relies on physiologically-realistic mechanisms. Namely, the

framework of mathematical relationships between inter-related MN-specific properties (Fig. 4E) ensures MN-specificity and maintains the parameters and predictions of the LIF model within physiological bounds defined by the available experimental data. Therefore, the method ensures obtaining a physiological distribution of the MN properties across the fully reconstructed MU pool consistent with Henneman's size principle (Henneman, 1981). For these reasons, reconstruction methods, such as that described in Fig. 4, are powerful tools for accurately describing the neural drive to muscle both at the MU-scale and the muscle-scale from limited samples of experimentally observed MUs.

4.3. Current limitations and future perspectives of MU pool reconstruction methods

Methods of experimental data augmentation for MU analysis have some limitations and potential for further developments. First, the accuracy of the neural drive estimated from the artificial full pool of MUs is to some extent sensitive to the quality of the observed sample of identified MUs. Reliable predictions of the full MU pool activity are obtained as long as the full MU pool is reconstructed from an experimental sample of MUs that are identified in each region of the recruitment range (Caillet et al., 2022b). Caillet (2023) demonstrated that as few as five experimental MUs regularly spread across the recruitment range are sufficient for deriving credible digital twins of the full pool and reliable estimates of the neural drive at muscle-scale. Of note, the original MU sample need not display an exponential distribution of thresholds for reliable data augmentation, as the method re-captures the exponential shape with the process in Fig. 4G, H. However, more representative samples of experimental MUs bring complementary information to the reconstruction process in Fig. 4G, H and yield more reliable predictions of the full MU pool activity (see Fig. 3, top-middle versus top-right subplots). Then, the accuracy of current data augmentation methods remains limited when the input experimental MUs are not identified over the full recruitment range. For example, the neural drive predicted by the full pool of artificial MUs remains inaccurate in the regions of low forces where identified MUs are often lacking, as discussed (bottom plots in Fig. 3). In such cases, the reconstructed MU pools display exponential MU distributions, contrary to the input samples of experimentally identified MUs, but receive non-physiological Common Current Input (Fig. 4C), that onset at the time of the earliest-recruited identified MU and is zero until that time. Consequently, applying the data augmentation method in Fig. 4 to an experimental MU sample is meaningful for deriving an estimate of the full MU activity, the reliability of which is only ensured if the original sample identified MUs in each range of recruitment.

A second limitation of current data augmentation methods is their sensitivity to the chosen force recruitment curve, as discussed by Caillet et al., 2022b. The properties of the recruitment curve determine the indexing of the experimental MUs into the full MU pool (Fig. 4B), which has consequences on the estimated continuous distribution of MN properties across the full MU pool (Fig. 4H) and the simulated discharge activity of the full MU pool (Fig. 4J). As the exponential shape and the range of MU recruitment are muscle-specific, the data augmentation methods should be applied with muscle-consistent models of recruitment curves, when available. Otherwise, the recruitment curve may also be calibrated by minimizing the difference between simulated and ground truth (normalized isometric force trace) neural drives at muscle-scale, as advised in Caillet et al., 2022b.

Third, the single-compartment LIF model with current synapses proposed in Fig. 4C provides accurate predictions of MN firing behaviour during isometric muscle contractions but comes with intrinsic limitations in physiological accuracy (Burkitt, 2006; Caillet et al., 2022b; Teeter et al., 2018). For example, the LIF model of Fig. 3 describes the physiological saturation of firing rates and follows the onion-skin scheme (De Luca & Hostage, 2010) with a phenomenological parameter estimated from the available experimental data. Rather, saturation may be described with more physiological accuracy with a single-compartment LIF model with lumped active conductances (Burkitt, 2006; Caillet et al., 2022b), where the intensity of the input current decreases with increasing membrane depolarization. Likewise, the changes in MN discharge patterns associated with dynamic muscle contractions may be phenomenologically captured with muscle state-related alterations to the properties of the single-compartment LIF model proposed in Fig. 4C. For example, rate modulation differs between concentric and eccentric contractions (Kossev & Christova, 1998; Christova & Kossev, 2000) but also varies with contraction speed (Desmedt & Godaux, 1978; Van Bolhuis et al., 1997). However, changes in MN discharge behaviour between isometric and dynamics contractions rely on changes in the intrinsic properties of MNs. For example, afferent feedback activity varies with muscle length (Pasquet et al., 2005) following an uneven distribution across the MN pool (Heckman & Enoka, 2012), synaptic input to the dendrites differs between isometric and anisometric contractions (Tax et al., 1989; Van Bolhuis et al., 1997), and the amplitude of dendritic persistent inward currents varies with changes in limb position and joint angle (Hyngstrom et al., 2007). Therefore, these electrophysiological mechanisms and changes in MNs' intrinsic excitability would be more accurately captured by more advanced MN models, such two-compartment models with dendritic activity.

Fourth, the reconstructed full MU pools and their activity, although realistic, only remain estimates of the true physiological process. The predicted activity of the reconstructed pools is only validated, at the MU-scale, for the MUs identified experimentally. This leaves room for variation in the estimation of the other non-identified MUs, the predicted dynamics of which are only constrained by the validation of the neural drive at muscle-scale and the afore-discussed physiological laws implemented in the architecture of the model. Therefore, acceptable variations in the size N of the MU pool, the shape of the recruitment curve (Fig. 4B), the definition of the Common Current Input (Fig. 4C), the definition of the MN-specific mathematical relationships (Fig. 4E), or the calibration and reconstruction methods (Fig. 4F, G) may yield, for the same input sample, different estimates of reconstructed MU pools that return similar validation results. For example, the data augmentation method in Fig. 4 is not sensitive to the chosen value of N (size of the full MU pool) and the neural drive at muscle-scale may be successfully validated with reconstructed pools of physiological numbers of MUs ($N = 400$ for the TA) or with reduced pools of as few as 10 MUs (Caillet et al., 2022b). While further research should be pursued on the numerosity of these possible multiple solutions, this limitation does not revoke that the reconstructed pool and its activity as output by the data augmentation method is likely to be a realistic description of the true neural drive to muscle.

Finally, it is relevant to note that the concepts and methods presented in this section and in Fig. 4 relates to a single pool of MN that receives one source of common synaptic input. However, the same approaches can be extended in a straightforward way to multiple groups/pools of motor neurons, each receiving different sources of common input (Hug et al., 2023). In this case, once the separate groups of MNs are identified as each receiving common input, the MNs would be modelled by separate cohorts of MN LIF models.

5. Neuromechanics: Predicting forces from accurate decoding of the neural drive

We reviewed experimental and computational methods to observe the behaviour of discharging MUs that provide accurate estimates of the neural drive to muscle during human muscle contractions. These identification methods are of particular importance for studies that aim to decode muscle function from neural intent, i.e. neuromechanical investigations on how the neural commands determine behaviour.

5.1. Single-input single-output EMG-driven predictions of force

Traditionally, computational simulations of human muscle contractions are performed with EMG-driven Hill-type models of whole muscles (Hof & Van Den Berg, 1981; Lloyd & Besier, 2003; Pizzolato et al., 2015; Caillet et al., 2022c). In these methods, a single-actuator Hill-type muscle model phenomenologically transforms, in a single-input single-output strategy, the experimental EMG envelope into muscle force. This approach is well-established (Caillet et al., 2022c), and has had important applications, for example in human–machine interfacing (Sartori et al., 2012; Ao et al., 2017; Caggiano et al., 2022; Cimolato et al., 2022). However, as discussed above, EMG envelopes provide only a crude description of the neural drive to muscle, so that force predictions and neuromechanical analyses are limited with this approach. As an example, because of lack of accuracy, it is not possible with this approach to analyse the effect of MU synchronization on the steadiness of a task (Thompson et al., 2018).

To address the limitations of classic EMG-driven models, some studies (Sartori et al., 2017; Thompson et al., 2018; Kapelner et al., 2020) replaced the EMG envelope with a more accurate description of the neural drive, that is the filtered cumulative spike train (fCST) computed from discharging MUs identified from decomposed HDEMG signals. Yet, in both the global EMG- and fCST-driven approaches, the recruitment and discharge dynamics of the active MU pool are lumped into a single phenomenological macroscopic neural control signal. These single-input single-output strategies therefore maintain muscle modelling at the macroscopic level rather than describing the force-generating process at the level of individual MUs. This hinders the investigation of human neuromuscular control with computational tools.

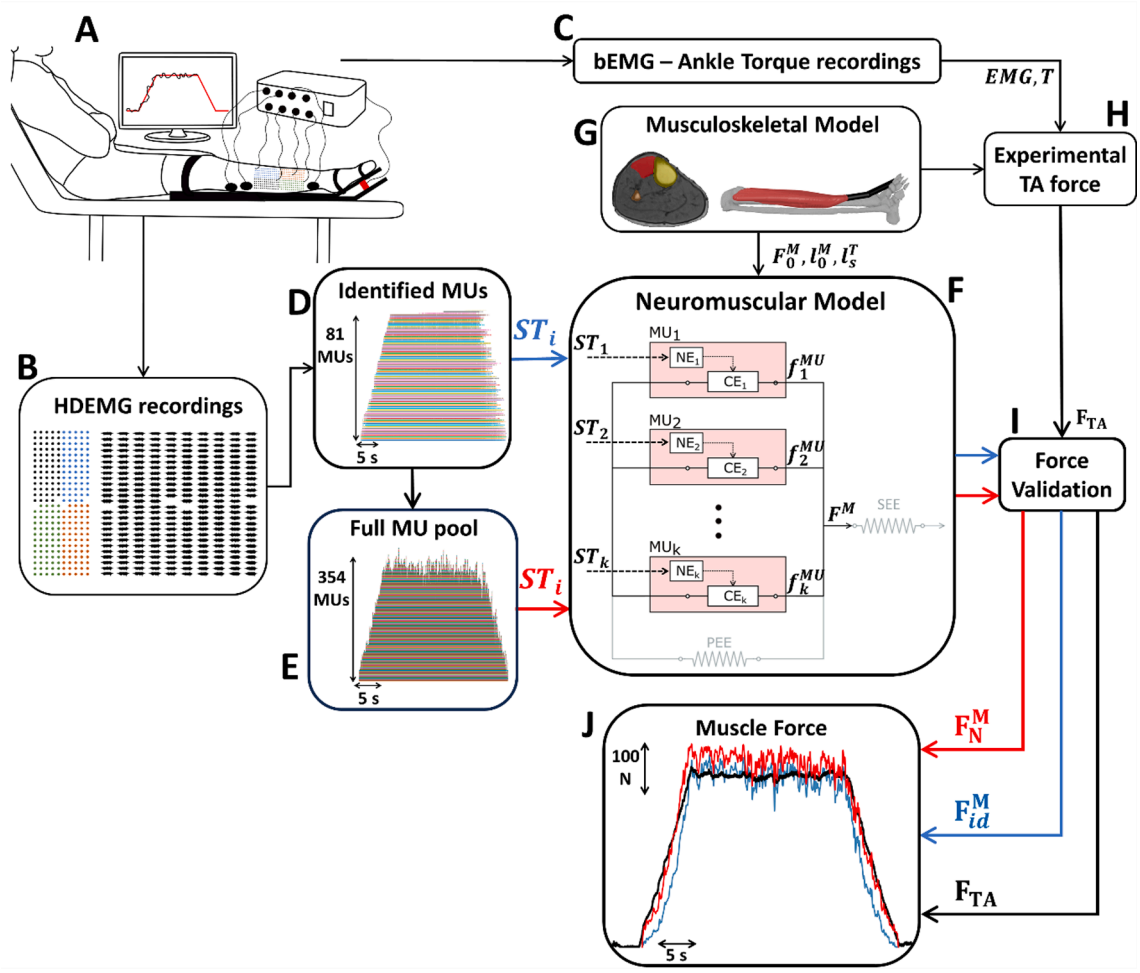

Fig. 5. Computational method for predicting whole muscle forces from motoneuronal spiking activity using a motoneuron (MN)-driven computational muscle model with motor unit (MU) resolution. (A-C) In Caillet et al., (2023a), high-density electromyographic (HDEMG) signals were recorded from the tibialis anterior (TA) muscle during isometric trapezoidal dorsiflexion. The ankle torque T and four bipolar EMG (bEMG) signals from co-contracting muscles were also recorded. (D) The HDEMG signals were decomposed into spike trains ($ST_i, i \in [\![1;81]\!]$) for 81 identified MUs in this example. (E) The discharge activity of the full pool of active MUs ($ST_i, i \in [\![1;354]\!]$) was generated from the 81 identified spike trains with the computational method in Fig. 4. (F) A MN-driven neuromuscular model with MU resolution transforms the spike trains derived previously ($ST_1, ST_2, \cdots, ST_k$) into MU forces $\left(f_1^{MU}, f_2^{MU}, \cdots, f_k^{MU}\right)$, that sum into the predicted whole muscle force F^M. Here, $k = 81$ or $k = 354$ whether the neuromuscular model receives the spike trains from the experimental sample of identified MUs (blue arrow) or from the full pool of artificial MUs (red arrow). The neuromuscular model describes the activation and contraction dynamics of each modelled MU with dedicated Neural Element (NE) and Contractile Element (CE). The passive dynamics of the parallel and in-series elastic elements (PEE and SEE) are neglected in Caillet et al., (2023a). In this approach, the neuromuscular model receives a subject-specific MU-specific neural control. (G) A subject-specific musculoskeletal model, derived from segmented medical images, provides further subject-specific muscle-specific architectural parameters (F_0^M, l_0^M, l_s^T) to couple with the neuromuscular model. (H) The subject-specific musculoskeletal model, the recorded ankle, and the bEMG signals recorded from co-contracting muscles are used to estimate the experimental force F_{TA} generated by the TA muscle (Caillet et al., 2023a). (I-J) The muscle force predicted from the experimental sample of identified MUs (F_{id}^M, blue arrow and trace) and from the full pool of artificial MUs (F_N^M, red arrow and trace) are validated against the experimental muscle force (F_{TA}, black arrow and trace).

5.2. Motoneuron-driven models of muscle force

In response to the limitations of single-input strategies, Caillet et al., (2023a) developed a neuromuscular model that comprehensively describes the force-generating dynamics of individual MUs. This method is summarised in Fig. 5. A cohort of Hill-type models transforms an input vector of MN spike trains (Fig. 5D,E) derived from HDEMG (Fig. 5A, B) into an output vector of individual MU forces (Fig. 5F), that sum into the predicted whole muscle force (Fig. 5J). Models of MU pools were previously proposed (Hatze, 1978; Hatze, 1980; Fuglevand et al., 1993; Raikova et al., 2018; Carriou et al., 2019), but all were used in combination with an artificial (not data-driven) neural drive. In Fig. 5, the neuromuscular model receives processed HDEMG data and was tested both with MU samples identified from HDEMG (Fig. 5B,D) and full pool of artificial MUs (Fig. 5E) obtained with the reconstruction method presented in Fig. 4. These approaches were tested (Caillet et al., 2023a) for trapezoidal contractions of the TA muscle up to 30 % and 50 % MVC with three grids of varying interelectrode distance (as in Fig. 3). An open-source implementation of this approach is publicly available at https://github.com/ArnaultCAILLET/MN-driven-Neuromuscular-Model-with-motor-unit-resolution. Across all conditions, the accuracy in predicting muscle force (Fig. 5H, I) systematically increased, especially in the regions of low forces, with greater numbers of electrodes, denser grids of electrodes, with the full pool of artificial MUs obtained by data augmentation (red trace in Fig. 5J) versus the experimental MU sample (blue trace in Fig. 5J), and at 30 % MVC versus 50 % MVC. These results echo with the conclusions previously drawn and stress the importance of deriving an input representative MU population, i.e., experimentally sampling the MU pool in a representative way, for controlling MN-driven neuromuscular models with realistic neural drive. In particular, neglecting the discharge activity of low-threshold MUs results in ignoring the force-generating contribution of those MUs to the whole muscle force, that is underpredicted at low contraction intensities. Limited samples of identified MUs (e.g., samples of 2–22 MUs used in another model of MU pool (Gogeascoechea et al., 2023)), which likely over-represent the activity of high-threshold MUs, are therefore unfit for accurately controlling models of a MU pool directly. This is why in cases of limited MU samples, the unexplained EMG residual is added to the fCST after parameter calibration in fCST-driven approaches (Sartori et al., 2017). As a final note, MN-driven models with MU resolution provide a more physiologically accurate description of the force-generating dynamics of muscles than traditional single-input single-output EMG-driven models. The functioning of traditional EMG-driven models relies on phenomenological non-linear transformations, like between EMG and compound "muscle activation", that include phenomenological parameters that cannot be experimentally estimated and must be calibrated to achieve prediction accuracy, usually by matching estimated and ground truth joint moments. Parameter calibration yields a risk of parameter over-fitting when the calibration set is small and lacks a large variety of motor tasks, so that EMG-driven models may not perform well on test sets that include different trials of motor task (Caillet, 2023). Conversely, MN-driven models with MU resolution may integrate parameters that have a physiological meaning and may be measured experimentally, so that parameter calibration is avoided. For example, Caillet et al., (2023a) proposed advanced physiological models of the MUs' activation dynamics, where changes in action potential firing modulates the fusion of the cascading twitches of free calcium ion concentration, calcium-troponin concentration, and normalized MU activation. As the parameters governing these cascading twitch models could be directly identified from recent experimental data, Caillet et al., (2023a) proposed distributing the twitch properties of these models across the MU pool (peak amplitude, time-to-peak, half relaxation time) by modelling different dynamics for low-threshold and high-threshold MUs. As a result of this physiological approach, acceptable twitch fusion to tetanus was observed for the modelled MUs and discussed in Caillet et al., (2023a), so that the resulting fused MU normalized forces, scaled with a distribution of the MUs' maximum forces across the MU pool derived from the literature, achieved accurate estimations of the total muscle force without having to rely at any point on steps of parameter calibration.

6. Conclusions and perspectives

The neural drive to muscle refers to the discharge activity of the active motoneuron pool, i.e., to the ensemble of action potentials transmitted to the muscle fibres and responsible for muscle force generation. The neural drive to muscles is the ultimate signal for muscle control; its accurate estimate is necessary for establishing its physiological link with the resulting muscle forces for the neuromechanical investigation of movement. Accurately identifying the neural drive to muscle in humans *in vivo* is however challenging. The MU samples identified from decomposed EMG signals usually include relatively few identified MUs, lack the activity of low-threshold MUs, and over-represent high-threshold MUs, so that they are inaccurate descriptions of the active MU pool. Here, we reviewed electrophysiological methods to estimate larger samples of MUs that follow a physiological exponential distribution across the MU pool's recruitment range, i.e., many low-threshold and few high-threshold MUs (Fig. 2). These improvements are obtained by increasing the number and density of surface or intramuscular EMG electrodes (Fig. 3). Then, we described how a reliable estimation of the discharge activity of the full MU pool can be reconstructed with computational data augmentation methods from the optimized – but still limited – experimental data (Fig. 4).

The accurate and comprehensive description of the neural drive to muscle from individual motoneuronal activity finds crucial applications in the control of neuromuscular models (Fig. 5), but also in the investigation of neural control strategies, including the study of neural synergies (Hug et al., 2023) and functional connectivity (Bräcklein et al., 2022), in clinical applications with the diagnosis and monitoring of neurophysiological disorders (Kelly et al., 2023; Bashford et al., 2020), or in neurorehabilitation technologies, e.g., for tremor suppression (Puttaraksa et al., 2022), prosthetics control (Farina et al., 2017; Farina et al., 2021), and assistive exoskeleton control (Jung et al., 2021).

Funding resources

Dario Farina is supported by the European Research Council Synergy Grant NaturalBionicS (contract #810346), the EPSRC Transformative Healthcare, NISNEM Technology (EP/T020970), and the BBSRC, "Neural Commands for Fast Movements in the Primate Motor System" (NU-003743). Luca Modenese is supported by a Scientia Fellowship from the University of New South Wales, Australia. The funders had no role in study design, data collection and analysis, decision to publish, or preparation of the manuscript.

Declaration of competing interest

The authors declare that they have no known competing financial interests or personal relationships that could have appeared to influence the work reported in this paper.

References

Afsharipour, B., Soedirdjo, S., Merletti, R., 2019. Two-dimensional surface EMG: the effects of electrode size, interelectrode distance and image truncation. Biomed. Signal Process. Control 49, 298–307.

Ao, D., Song, R., Gao, J., 2017. Movement performance of human-robot cooperation control based on EMG-driven hill-type and proportional models for an ankle power-assist exoskeleton robot. TNSRE 25, 1125–1134.

Avrillon, S., Hug, F., Gibbs, C., Farina, D., 2023b. Tutorial on MUedit: An open-source software for identifying and analysing the discharge timing of motor units from electromyographic signals. bioRxiv 2023.07. 13.548568. https://doi.org/10.1101/2023.07.13.548568.

Avrillon, S., Hug, E., Caillet, F., 2023a. The decoding of extensive samples of motor units in human muscles reveals the rate coding of whole motoneuron pools. Biorxiv. https://doi.org/10.1101/2023.11.25.568607.
Bashford, J., Mills, K., Shaw, C., 2020. The evolving role of surface electromyography in amyotrophic lateral sclerosis: a systematic review. Clin. Neurophysiol. 131 (4), 942–950.
Bennett, D.J., Hultborn, H., Fedirchuk, B., Gorassini, M., 1998. Synaptic activation of plateaus in hindlimb motoneurons of decerebrate cats. J. Neurophysiol. 80, 2023–2037.
Besomi, M., Hodges, P.W., Van Dieën, J., Carson, R.G., Clancy, E.A., Disselhorst-Klug, C., Holobar, A., Hug, F., Kiernan, M.C., Lowery, M., 2019. Consensus for experimental design in electromyography (CEDE) project: electrode selection matrix. J. Electromyogr. Kinesiol. 48, 128–144.
Besomi, M., Hodges, P.W., Clancy, E.A., Van Dieën, J., Hug, F., Lowery, M., Merletti, R., Søgaard, K., Wrigley, T., Besier, T., 2020. Consensus for experimental design in electromyography (CEDE) project: amplitude normalization matrix. J. Electromyogr. Kinesiol. 53, 102438.
Bhattacharyya, A., 1943. On a measure of divergence between two statistical populations defined by their probability distribution. Bull. Calcutta Math. Soc. 35, 99–110.
Binder, M.D., Heckman, C.J., Powers, R.K., 1996. The physiological control of motoneuron activity. In: Rowell LB, S.J. (Ed.), Handbook of Physiology: Exercise, Regulation and Integration of Multiple Systems. New York: Oxford Univ Press, pp. 3–53.
Binder, M.D., Powers, R.K., Heckman, C.J., 2020. Nonlinear input-output functions of motoneurons. Physiology 35, 31–39.
Bräcklein, M., Barsakcioglu, D.Y., Del Vecchio, A., Ibáñez, J., Farina, D., 2022. Reading and modulating cortical β bursts from motor unit spiking activity. J. Neurosci. 42, 3611–3621.
Burke, R.E., 1981. Motor units: anatomy, physiology, and functional organization. In: Brooks, V.B. (Ed.), Handbook of Physiology, the Nervous System. American Physiological Society, Motor Control, pp. 345–422.
Burkitt, A.N., 2006. A review of the integrate-and-fire neuron model: I. homogeneous synaptic input. Biol. Cybern. 95, 1–19.
Caggiano, V., Wang, H., Durandau, G., Sartori, M., Kumar, V., 2022. MyoSuite–A contact-rich simulation suite for musculoskeletal motor control. arXiv preprint arXiv: 2205.13600 .
Caillet AH, Phillips AT, Carty C, Farina D, Modenese L (2022c) Hill-type computational models of muscle-tendon actuators: A systematic review. bioRxiv, doi: https://doi.org/10.1101/2022.10.14.512218.
Caillet, A.H., Avrillon, S., Kundu, A., Yu, T., Andrew, T.M., Phillips, Modenese, L., Farina, D., 2023b. Larger and denser: an optimal design for surface grids of EMG electrodes to identify greater and more representative samples of motor units. eNeuro ENEURO.0064-23.2023.
Caillet, A.H., Phillips, A.T., Farina, D., Modenese, L., 2022b. Estimation of the firing behaviour of a complete motoneuron pool by combining electromyography signal decomposition and realistic motoneuron modelling. PLoS Comput. Biol. 18, e1010556.
Caillet, A.H., Phillips, A.T., Farina, D., Modenese, L., 2022a. Mathematical relationships between spinal motoneuron properties. Life 11, e76489.
Caillet, A.H., Phillips, A.T.M., Farina, D., Modenese, L., 2023a. Motoneuron-driven computational muscle modelling with motor unit resolution and subject-specific musculoskeletal anatomy. PLoS Comput. Biol. 19, e1011606.
Caillet, A.H., 2023. Neuromuscular modelling of skeletal muscle contraction from experimental motoneuronal activity. PhD Thesis, Imperial College London, Chapters 3&4.
Carriou, V., Boudaoud, S., Laforet, J., Mendes, A., Canon, F., Guiraud, D., 2019. Multiscale hill-type modeling of the mechanical muscle behavior driven by the neural drive in isometric conditions. Comput. Biol. Med. 115, 103480.
Christova, P., Kossev, A., 2000. Human motor unit activity during concentric and eccentric movements. Electromyogr. Clin. Neurophysiol. 40 (6), 331–338.
Chung, B., Zia, M., Thomas, K.A., Michaels, J.A., Jacob, A., Pack, A., Sober, S.J., 2023. Myomatrix arrays for high-definition muscle recording. Elife 12, RP88551.
Cimolato, A., Driessen, J.J., Mattos, L.S., De Momi, E., Laffranchi, M., De Michieli, L., 2022. EMG-driven control in lower limb prostheses: a topic-based systematic review. J. Neuroeng. Rehabil. 19, 1–26.
Cisi, R.R.L., Kohn, A.F., 2008. Simulation system of spinal cord motor nuclei and associated nerves and muscles, in a web-based architecture. J. Comput. Neurosci. 25, 520–542.
Clancy, E.A., Morin, E.L., Hajian, G., Merletti, R., 2023. Tutorial. surface electromyogram (sEMG) amplitude estimation: best practices. J. Electromyogr. Kinesiol. 72:102807.
Clarke, A.K., Atashzar, S.F., Del Vecchio, A., Barsakcioglu, D., Muceli, S., Bentley, P., Urh, F., Holobar, A., Farina, D., 2020. Deep learning for robust decomposition of high-density surface EMG signals. IEEE Trans. Biomed. Eng. 68, 526–534.
D'Avella, A., Bizzi, E., 2005. Shared and specific muscle synergies in natural motor behaviors. PNAS 102 (8), 3076–3081.
De Luca, C.J., 1997. The use of surface electromyography in biomechanics. J. Appl. Biomech. 13, 135–163.
De Luca, C.J., Hostage, E.C., 2010. Relationship between firing rate and recruitment threshold of motoneurons in voluntary isometric contractions. J. Neurophysiol. 104, 1034–1046.
Del Vecchio, A., Holobar, A., Falla, D., Felici, F., Enoka, R.M., Farina, D., 2020. Tutorial: analysis of motor unit discharge characteristics from high-density surface EMG signals. J. Electromyogr. Kinesiol. 53, 102426.
Dengler, R., Stein, R.B., Thomas, C.K., 1988. Axonal conduction velocity and force of single human motor units. Muscle Nerve: Off. J. Am. Assoc. Electrodiagnostic Med. 11 (2), 136–145.
Desmedt, J.E., Godaux, E., 1978. Ballistic contractions in fast or slow human muscles; discharge patterns of single motor units. J. Physiol. 285 (1), 185–196.
Dideriksen, J.L., Farina, D., Baekgaard, M., Enoka, R.M., 2010. An integrative model of motor unit activity during sustained submaximal contractions. J. Appl. Physiol. 108, 1550–1562.
Dideriksen, J.L., Enoka, R.M., Farina, D., 2011. Neuromuscular adjustments that constrain submaximal EMG amplitude at task failure of sustained isometric contractions. J. Appl. Physiol. 111, 485–494.
Duchateau, J., Enoka, R.M., 2022. Distribution of motor unit properties across human muscles. J. Appl. Physiol. 132, 1–13.
Duchateau, J., Hainaut, K., 1990. Effects of immobilization on contractile properties, recruitment and firing rates of human motor units. J. Physiol. 422 (1), 55–65.
Enoka, R.M., Duchateau, J., 2017. Rate coding and the control of muscle force. Cold Spring Harbor Perspect. Med. 7.
Enoka, R.M., Farina, D., 2021. Force steadiness: from motor units to voluntary actions. Physiology 36, 114–130.
Enoka, R.M., Fuglevand, A.J., 2001. Motor unit physiology: some unresolved issues. Muscle Nerve: Off. J. Am. Assoc. Electrodiagnostic Med. 24 (1), 4–17.
Farina, D., Holobar, A., 2016. Characterization of human motor units from surface EMG decomposition. Proc IEEE 104, 353–373.
Farina, D., Negro, F., 2015. Common synaptic input to motor neurons, motor unit synchronization, and force control. Exerc. Sport Sci. Rev. 43, 23–33.
Farina, D., Merletti, R., Enoka, R.M., 2004. The extraction of neural strategies from the surface EMG. J. Appl. Physiol. 96, 1486–1495.
Farina, D., Merletti, R., Enoka, R.M., 2014a. The extraction of neural strategies from the surface EMG: an update. J. Appl. Physiol. 117, 1215–1230.
Farina, D., Negro, F., Dideriksen, J.L., 2014b. The effective neural drive to muscles is the common synaptic input to motor neurons. J. Physiol. 592, 3427–3441.
Farina, D., Vujaklija, I., Sartori, M., Kapelner, T., Negro, F., Jiang, N., Bergmeister, K., Andalib, A., Principe, J., Aszmann, O.C., 2017. Man/machine interface based on the discharge timings of spinal motor neurons after targeted muscle reinnervation. Nat. Biomed. Eng. 1, 1–12.
Farina, D., Vujaklija, I., Brånemark, R., Bull, A.M.J., Dietl, H., Graimann, B., Hargrove, L. J., Hoffmann, K., Huang, H., Ingvarsson, T., Janusson, H.B., Kristjánsson, K., Kuiken, T., Micera, S., Stieglitz, T., Sturma, A., Tyler, D., Weir, R.F., Aszmann, O.C., 2021. Toward higher-performance bionic limbs for wider clinical use. Nat. Biomed. Eng. 1–13.
Feiereisen, P., Duchateau, J., Hainaut, K., 1997. Motor unit recruitment order during voluntary and electrically induced contractions in the tibialis anterior. Exp. Brain Res. 114 (1), 117–123. https://doi.org/10.1007/pl00005610. PMID: 9125456.
Fuglevand, A.J., Winter, D.A., Patla, A.E., 1993. Models of recruitment and rate coding organization in motor-unit pools. J. Neurophysiol. 70, 2470–2488.
Gallina, A., Disselhorst-Klug, C., Farina, D., Merletti, R., Besomi, M., Holobar, A., Enoka, R.M., Hug, F., Falla, D., Søgaard, K., 2022. Consensus for experimental design in electromyography (CEDE) project: high-density surface electromyography matrix. J. Electromyogr. Kinesiol. 64, 102656.
Glaser, V., Holobar, A., 2018. Motor unit identification from high-density surface electromyograms in repeated dynamic muscle contractions. IEEE Trans. Neural Syst. Rehabil. Eng. 27, 66–75. PMID:30571641.
Gogeascoechea, A., Ornelas-Kobayashi, R., Yavuz, U.S., Sartori, M., 2023. Characterization of motor unit firing and twitch properties for decoding musculoskeletal force in the human ankle joint in vivo. IEEE Trans. Neural Syst. Rehabil. Eng.
Goldberg, L.J., Derfler, B., 1977. Relationship among recruitment order, spike amplitude, and twitch tension of single motor units in human masseter muscle. J. Neurophysiol. 40 (4), 879–890.
Hatze, H., 1978. A general myocybernetic control model of skeletal muscle. Biol. Cybern. 28, 143–157.
Hatze, H., 1980. Myocybernetic Control Models of Skeletal Muscle - Characteristics and Applications. University of South Africa Press, Pretoria.
Heckman, C.J., Enoka, R.M., 2004. Physiology of the motor neuron and the motor unit. In Anonymous Handbook of Clinical Neurophysiology. Elsevier, pp. 119–147.
Heckman, C.J., Enoka, R.M., 2012. Motor Unit. Compr. Physiol. 2, 2629–2682.
Henneman, E., 1957. Relation between size of neurons and their susceptibility to discharge. Science 126, 1345–1347.
Henneman, E., 1981. Recruitment of motoneurons: the size principle. Motor Unit Types, Recruitment and Plasticity in Health and Disease 26–60.
Hof, A.L., Van den Berg, J.W., 1981. EMG to force processing I: an electrical analogue of the Hill muscle model. J. Biomech. 14 (11), 747–758.
Holobar, A., Farina, D., 2014. Blind source identification from the multichannel surface electromyogram. PM 35, R143–R165.
Hug, F., Avrillon, S., Del Vecchio, A., Casolo, A., Ibanez, J., Nuccio, S., Rossato, J., Holobar, A., Farina, D., 2021a. Analysis of motor unit spike trains estimated from high-density surface electromyography is highly reliable across operators. J. Electromyogr. Kinesiol. 58, 102548.
Hug, F., Del Vecchio, A., Avrillon, S., Farina, D., Tucker, K., 2021b. Muscles from the same muscle group do not necessarily share common drive: evidence from the human triceps surae. J. Appl. Physiol. 130, 342–354.
Hug, F., Avrillon, S., Ibáñez, J., Farina, D., 2023. Common synaptic input, synergies and size principle: control of spinal motor neurons for movement generation. J. Physiol. (lond.) 601, 11–20.
Hyngstrom, A.S., Johnson, M.D., Miller, J.F., Heckman, C.J., 2007. Intrinsic electrical properties of spinal motoneurons vary with joint angle. Nat. Neurosci. 10 (3), 363–369.

Jenz, S.T., Beauchamp, J.A., Gomes, M.M., Negro, F., Heckman, C.J., Pearcey, G.E., 2023. Estimates of persistent inward currents in lower limb motoneurons are larger in females than in males. J. Neurophysiol. 129, 1322–1333.
Jung, M.K., Muceli, S., Rodrigues, C., Megía-García, Á., Pascual-Valdunciel, A., Del-Ama, A.J., Gil-Agudo, A., Moreno, J.C., Barroso, F.O., Pons, J.L., 2021. Intramuscular EMG-driven musculoskeletal modelling: Towards implanted muscle interfacing in spinal cord injury patients. IEEE Trans. Biomed. Eng. 69, 63–74.
Kapelner, T., Vujaklija, I., Jiang, N., Negro, F., Aszmann, O.C., Principe, J., Farina, D., 2019. Predicting wrist kinematics from motor unit discharge timings for the control of active prostheses. J. Neuroeng. Rehabil. 16 (1), 1–11.
Kapelner, T., Sartori, M., Negro, F., Farina, D., 2020. Neuro-musculoskeletal mapping for man-machine interfacing. Sci. Rep. 10, 1–10.
Kelly, K.M., Mizell, J., Bigdeli, L., Paul, S., Tellez, M.A., Bartlett, A., Arnold, W.D., 2023. Differential impact on motor unit characteristics across severities of adult spinal muscular atrophy. Ann. Clin. Transl. Neurol. 10 (12), 2208–2222.
Kernell, D., 2006. The Motoneurone and its Muscle Fibres. Oxford University Press UK.
Kossev, A., Christova, P., 1998. Discharge pattern of human motor units during dynamic concentric and eccentric contractions. Electroencephalogr Clin Neurophysiol/Electromyogr Motor Control 109 (3), 245–255.
Kukulka, C.G., Clamann, H.P., 1981. Comparison of the recruitment and discharge properties of motor units in human brachial biceps and adductor pollicis during isometric contractions. Brain Res. 219 (1), 45–55.
Lee, R.H., Heckman, C.J., 1998. Bistability in spinal motoneurons in vivo: systematic variations in rhythmic firing patterns. J. Neurophysiol. 80, 572–582. https://doi.org/10.1152/jn.1998.80.2.572.
Lee, R.H., Kuo, J.J., Jiang, M.C., Heckman, C.J., 2003. Influence of active dendritic currents on input-output processing in spinal motoneurons in vivo. J. Neurophysiol. 89, 27–39.
Lloyd, D.G., Besier, T.F., 2003. An EMG-driven musculoskeletal model to estimate muscle forces and knee joint moments in vivo. J. Biomech. 36, 765–776.
Lloyd, D.G., Jonkers, I., Delp, S.L., Modenese, L., 2023. The history and future of neuromusculoskeletal biomechanics. J. Appl. Biomech. 39 (5), 273–283.
Luca, D.e., 2006. Adam, Wotiz, Gilmore, Nawab, decomposition of surface EMG signals. J Neurophysiol 96, 1646–1657.
Martinez-Valdes, E., Enoka, R.M., Holobar, A., McGill, K., Farina, D., Besomi, M., Hug, F., Falla, D., Carson, R.G., Clancy, E.A., 2023. Consensus for experimental design in electromyography (CEDE) project: single motor unit matrix. J. Electromyogr. Kinesiol. 68, 102726.
Merletti, R., Cerone, G.L., 2020. Tutorial. surface EMG detection, conditioning and pre-processing: best practices. J. Electromyogr. Kinesiol. 54:102440.
Merletti, R., Muceli, S., 2019. Tutorial. surface EMG detection in space and time: best practices. J. Electromyogr. Kinesiol. 49:102363.
Milner-Brown, H.S., Stein, R.B., Yemm, R., 1973. Changes in firing rate of human motor units during linearly changing voluntary contractions. J Physiol 230, 371–390.
Monster, A.W., Chan, H.I.N.G., 1977. Isometric force production by motor units of extensor digitorum communis muscle in man. J. Neurophysiol. 40 (6), 1432–1443.
Muceli, S., Poppendieck, W., Negro, F., Yoshida, K., Hoffmann, K.P., Butler, J.E., Gandevia, S.C., Farina, D., 2015. Accurate and representative decoding of the neural drive to muscles in humans with multi-channel intramuscular thin-film electrodes. J. Physiol. (Lond.) 593, 3789–3804.
Muceli, S., Poppendieck, W., Holobar, A., Gandevia, S., Liebetanz, D., Farina, D., 2022. Blind identification of the spinal cord output in humans with high-density electrode arrays implanted in muscles. Sci. Adv. 8, eabo5040.
Nawab, C., Luca, D.e., 2010. High-yield decomposition of surface EMG signals. Clin. Neurophysiol. 121, 1602–1615.
Negro, F., Farina, D., 2011. Decorrelation of cortical inputs and motoneuron output. J. Neurophysiol. 106, 2688–2697.
Negro, F., Muceli, S., Castronovo, A.M., Holobar, A., Farina, D., 2016. Multi-channel intramuscular and surface EMG decomposition by convolutive blind source separation. JNE 13, 026027.
Oliveira, A.S., Negro, F., 2021. Neural control of matched motor units during muscle shortening and lengthening at increasing velocities. J. Appl. Physiol. 130, 1798–1813. PMID:33955258.
Ornelas-Kobayashi, R., Gogeascoechea, A., Sartori, M., 2023. Person-specific biophysical modeling of alpha-motoneuron pools driven by in vivo decoded neural synaptic input. IEEE Trans. Neural Syst. Rehabil. Eng. 31, 1532–1541.
Pasquet, B., Carpentier, A., Duchateau, J., 2005. Change in muscle fascicle length influences the recruitment and discharge rate of motor units during isometric contractions. J. Neurophysiol. 94 (5), 3126–3133.
Pizzolato, C., Lloyd, D.G., Sartori, M., Ceseracciu, E., Besier, T.F., Fregly, B.J., Reggiani, M., 2015. CEINMS: a toolbox to investigate the influence of different neural control solutions on the prediction of muscle excitation and joint moments during dynamic motor tasks. J. Biomech. 48 (14), 3929–3936.
Potvin, J.R., Fuglevand, A.J., 2017. A motor unit-based model of muscle fatigue. PLoS Comput. Biol. 13, e1005581.
Powers, R.K., Binder, M.D., 2001. Input-output functions of mammalian motoneurons. Rev. Physiol. Biochem. Pharmacol. 143, 137–263.
Powers, R.K., Heckman, C.J., 2017. Synaptic control of the shape of the motoneuron pool input-output function. J. Neurophysiol. 117, 1171–1184.
Puttaraksa, G., Muceli, S., Barsakcioglu, D.Y., Holobar, A., Clarke, A.K., Charles, S.K., Pons, J.L., Farina, D., 2022. Online tracking of the phase difference between neural drives to antagonist muscle pairs in essential tremor patients. IEEE Trans. Neural Syst. Rehabil. Eng. 30, 709–718.
Raikova, R., Celichowski, J., Angelova, S., Krutki, P., 2018. A model of the rat medial gastrocnemius muscle based on inputs to motoneurons and on an algorithm for prediction of the motor unit force. J. Neurophysiol. 120, 1973–1987.
Riek, S., Bawa, P., 1992. Recruitment of motor units in human forearm extensors. J. Neurophysiol. 68 (1), 100–108.
Romaiguère, P., Vedel, J.P., Pagni, S., Zenatti, A., 1989. Physiological properties of the motor units of the wrist extensor muscles in man. Exp. Brain Res. 78, 51–61.
Rossato, J., Hug, F., Tucker, K., Lacourpaille, L., Farina, D., Avrillon, S., 2023. I-spin live: An open-source software based on blind-source separation for decoding the activity of spinal alpha motor neurons in real-time. bioRxiv 2023.04. 14.536933, doi: https://doi.org/10.1101/2023.04.14.536933.
Sartori, M., Reggiani, M., Farina, D., Lloyd, D.G., 2012. EMG-driven forward-dynamic estimation of muscle force and joint moment about multiple degrees of freedom in the human lower extremity. PLoS One 7, e52618.
Sartori, M., Yavuz, U., Farina, D., 2017. In vivo neuromechanics: decoding causal motor neuron behavior with resulting musculoskeletal function. Sci. Rep. 7, 13465–113414.
Stephens, J.A., Usherwood, T.P., 1977. The mechanical properties of human motor units with special reference to their fatiguability and recruitment threshold. Brain Res. 125 (1), 91–97.
Tax, A.A.M., Van Der Gon, J.D., Gielen, C.C.A.M., Van den Tempel, C.M.M., 1989. Differences in the activation of m. biceps brachii in the control of slow isotonic movements and isometric contractions. Exp. Brain Res. 76, 55–63.
Teeter, C., Iyer, R., Menon, V., Gouwens, N., Feng, D., Berg, J., Szafer, A., Cain, N., Zeng, H., Hawrylycz, M., Koch, C., Mihalas, S., 2018. Generalized leaky integrate-and-fire models classify multiple neuron types. Nat. Commun. 9, 1–15.
Thompson, C.K., Negro, F., Johnson, M.D., Holmes, M.R., McPherson, L.M., Powers, R.K., Farina, D., Heckman, C.J., 2018. Robust and accurate decoding of motoneuron behaviour and prediction of the resulting force output. J. Physiol. (Lond.) 596, 2643–2659.
Valli, G., Ritsche, P., Casolo, A., Negro, F., De Vito, G., 2024. Tutorial: analysis of central and peripheral motor unit properties from decomposed high-density surface EMG signals with openhdemg. J. Electromyogr. Kinesiol. 74, 102850.
Van Bolhuis, B.M., Medendorp, W.P., Gielen, C.C.A.M., 1997. Motor unit firing behavior in human arm flexor muscles during sinusoidal isometric contractions and movements. Exp. Brain Res. 117, 120–130.
Van Cutsem, M., Duchateau, J., Hainaut, K., 1998. Changes in single motor unit behaviour contribute to the increase in contraction speed after dynamic training in humans. J. Physiol. 513 (1), 295–305.
Watanabe, R.N., Magalhães, F.H., Elias, L.A., Chaud, V.M., Mello, E.M., Kohn, A.F., 2013. Influences of premotoneuronal command statistics on the scaling of motor output variability during isometric plantar flexion. J. Neurophysiol. 110, 2592–2606.
Yeung, D., Negro, F., Vujaklija, I., 2023. Optimal motor unit subset selection for accurate motor intention decoding: towards dexterous real-time interfacing. IEEE Trans. Neural Syst. Rehabil. Eng.
Yokoyama, H., Sasaki, A., Kaneko, N., Saito, A., Nakazawa, K., 2021. Robust identification of motor unit discharges from high-density surface EMG in dynamic muscle contractions of the tibialis anterior. IEEE Access 9, 123901–123911.